THE 18th CHESAPEAKE SAILING YACHT SYMPOSIUM

ANNAPOLIS, MARYLAND, MARCH 2007

Database of Sail Shapes vs. Sail Performance and Validation of Numerical Calculation for Upwind Condition

Yutaka Masuyama, Kanazawa Institute of Technology, Japan
Yusuke Tahara, Osaka Prefecture University, Japan
Toichi Fukasawa, Kanazawa Institute of Technology, Japan
Naotoshi Maeda, Graduate School of Engineering, Osaka Prefecture University, Japan

ABSTRACT

Database of full-scale three-dimensional sail shapes are presented with the aerodynamic coefficients for the upwind condition of IMS type sails. Three-dimensional shape data are used for the input of numerical calculations and the results are compared with the measured sail performance. The sail shapes and performance are measured using a sail dynamometer boat *Fujin*. The *Fujin* is a 34-foot LOA boat, in which load cells and charge coupled devices (CCD) cameras are installed to measure the sail forces and shapes simultaneously. The sailing conditions of the boat, such as boat speed, heel angle, wind speed, wind angle, and so on, are also measured. The tested sail configurations are as follows: mainsail with 130% jib, mainsail with 75% jib and mainsail alone. Sail shapes are measured at several height positions. The measured shape parameters are chord length, maximum draft, maximum draft position, entry angle at the luff and exit angle at the leech. From these parameters three-dimensional coordinates of the sails are calculated by interpolation. These three-dimensional coordinates are tabulated with the aerodynamic coefficients.

Numerical calculations are performed using the measured sail shapes. The calculation methods are of two types; Reynolds-averaged Navier-Stokes (RANS)-based CFD and vortex lattice methods (VLM). A multi-block RANS-based CFD method was developed by one of the authors and is capable of predicting viscous flows and aerodynamic forces for complicated sail configuration for upwind as well as downwind conditions. Important features of the numerical method are summarized as follows: a Finite- Analytic scheme to discretize transport equations, a PISO type velocity-pressure coupling scheme, multi-block domain decomposition capability, and several choices of turbulence models depending on flows of interest. An automatic grid generation scheme is also included. Another calculation method, the vortex lattice method is also adopted. In this case, step-by-step calculations are conducted to attain the steady state of the sail in steady wind. Wake vortices are generated step-by-step, which flow in the direction of the local velocity vector. These calculated sail forces are compared with the measured one, and the validity of the numerical method is studied. The sail shape database and comparison with numerical calculations will provide a good benchmark for the sail performance analysis of the upwind condition of IMS type sails.

NOTATION

S_A	Sail area [m^2]
U_A	Apparent wind speed [m/s]
V_B	Boat velocity [m/s]
X, Y	Force components along x and y-axis in body axes system [N]
K, N	Moments around x and z-axis in body axes system [N-m]
x_{CE}, z_{CE}	x and z coordinates of center of effort of sails [m]
γ_A	Apparent wind angle [deg]
ρ_a	Density of air [kg/m^3]

INTRODUCTION

As the study progress of CFD, many sail performance calculations have been carried out using CFD. However, the validation of calculated results is very difficult because it requires data such as sail shape, forces acting on the sails and wind conditions, all measured simultaneously. For the case of wind tunnel tests, the measurement of this data is relatively easy, but there are insufficient points to accurately model sail shape, and the effects of low Reynolds Number due to the small sail model. On the other hand, for the case of full-scale tests, the problems of accuracy of sail shape and Reynolds Number are diminished, but the measurement of forces acting on the sail is difficult. In order to measure the sail forces directly, Milgram et al. (1993) and

Masuyama et al. (1997) built full-scale boats which have a sail dynamometer system. Hochkirch et al. (1999) also built a full-scale dynamometer boat, but they focused on the hydrodynamic forces acting on the fin keel and rudder. Hence the aerodynamic forces acting on the sail were not reported.

The boat of Milgram (1993) was a pioneer in the sail dynamometer system and indicated effectiveness of the system. The system, named the MIT Sailing Dynamometer, is a 35-foot boat containing an internal frame connected to the hull by six load cells configured to measure all forces and moments acting on the sails. At the same time, the sail shapes were measured and used for the input data of CFD analyses. However, in the report the sail shape data and the relation between sail shape and performance are not mentioned.

Masuyama and Fukasawa were encouraged by Milgram's work, and built a sail dynamometer boat *Fujin*. The measurement system of sail forces and moments is similar to the MIT Sailing Dynamometer. The results using IMS type sail were reported in the previous paper (Masuyama et al. 1997), in which the sail performance variation was indicated with the change of apparent wind angle and mainsail draft. Numerical calculation using vortex lattice method developed by Fukasawa (1993) was also performed using measured sail shape.

In this report, including experimental results performed after the previous paper, the relation between sail shape and performance for the upwind condition are presented and the results are compared with the latest numerical calculation methods.

A RANS-based CFD method developed by Tahara is used to demonstrate validation of the method through detailed comparison with the present measurements. Detailed validation studies of the method have been done for transition of the method to industrial design field, through application to geometries and flows which are theoretically and/or experimentally well understood and/or well known test cases. For instance, Tahara (1996a, 1996b, 1999), Tahara, Ando (2000), Tahara, Wilson, Carrica (2005) and Tahara, Wilson, Carrica, Stern (2006) are related to the evaluation of accuracy in predicting ship viscous free-surface flow and propulsive performances; and Tahara, Stern, Himeno (2004), and Tahara, Tohyama, Katsui (2006) are for CFD-based ship-hull-form optimizations. Several extended applications were investigated as well, e.g., multiple sail design of America's Cup sailing boat (Tahara, Hayashi, 2003) and parachute design of Mars landing spacecraft (Tahara, 2006).

In fact, the present application of the RANS-based CFD method to sail flow calculations is a new challenge for CFD. The pros and cons of the approach in comparison to well-established potential-flow theory will be clarified. The authors believe that the present validation study will yield further motivation to enhance CFD technology along with the design applications with more detailed analysis of the sail flow, as focused in the present study.

SAIL PLAN AND DEFINITION OF COEFFICIENTS

Full-scale sail tests were performed using a sail dynamometer boat, *Fujin*. The *Fujin* was built originally for sail tests for the Japanese America's Cup challenger in 1994. *Fujin* is a 10.3m-long ocean cruiser and has a sail dynamometer system in the hull which can measure sail forces and moments directly.

For the test of IMS type sail, the sails were made using values of I, J, P and E indicated in Table 1. The rigging of the *Fujin* was originally designed for the IACC sail. The genoa of IACC sail is relatively small. Therefore, the longitudinal position of the jib rail track of the *Fujin* was located forward than that of the typical IMS racer. For this reason, the tests were performed using 130% jib, and 75% jib, and a full batten mainsail. The sails were made by North Sails Japan. Table 1 shows the principal dimensions of the boat and Table 2 shows the detailed measurements of sails. Figure 1 also shows the sail plan. The 75% jib has cut up foot as shown in Figure 1. In order to apply the automatic gridding scheme for the numerical calculation, the foot shape was replaced by dotted line for the calculation.

Aerodynamic coefficients and coordinates of center of effort of the sails are defined as follows:

$$C_X = \frac{X_S}{\frac{1}{2}\rho_a {U_A}^2 S_A}, \qquad C_Y = \frac{Y_S}{\frac{1}{2}\rho_a {U_A}^2 S_A}, \qquad (1)$$

$$x_{CE} = \frac{N_S}{Y_S}, \qquad z_{CE} = \frac{K_S}{Y_S}$$

where X_S and Y_S are force components along x and y axes of the boat respectively, and K_S and N_S are moments around x and z axes. x_{CE} and z_{CE} are x and z coordinates of center of effort of sails. The aerodynamic forces acting on the mast and rigging are included in the sail forces. The origin of coordinates is located at the aft face of the mast (x-direction), and the height of deck level at the "J" point (z-direction) as shown in Figure 1. It should be noted that when the boat heels the Y_S force component is not directed in horizontal plane but is directed normal to the mast.

Table 1 Principal dimensions of *Fujin*

HULL		
LOA	[m]	10.35
LWL	[m]	8.80
BMAX	[m]	3.37
BWL	[m]	2.64
Disp	[ton]	3.86
SAIL		
I	[m]	11.00
J	[m]	3.61
P	[m]	12.55
E	[m]	4.51

Table 2 Detailed measurements of sails

	Mainsail	130% Jib	75% Jib
Peak Height [m]	13.82	10.70	9.90
Luff Length [m]	12.50	11.45	10.60
Foot Length [m]	4.44	4.89	* 3.16
Sail Area [m^2]	33.20	26.10	13.70
Height [%]	Chord Length [m]		
100	0.15	0.10	0.10
80	1.39	0.98	0.53
60	2.43	1.97	1.06
40	3.23	2.94	1.70
20	3.85	3.94	2.45
10	4.13	4.44	2.90
0	4.44	4.89	0.00

* Foot length of 75% jib indicates value at 5% height.

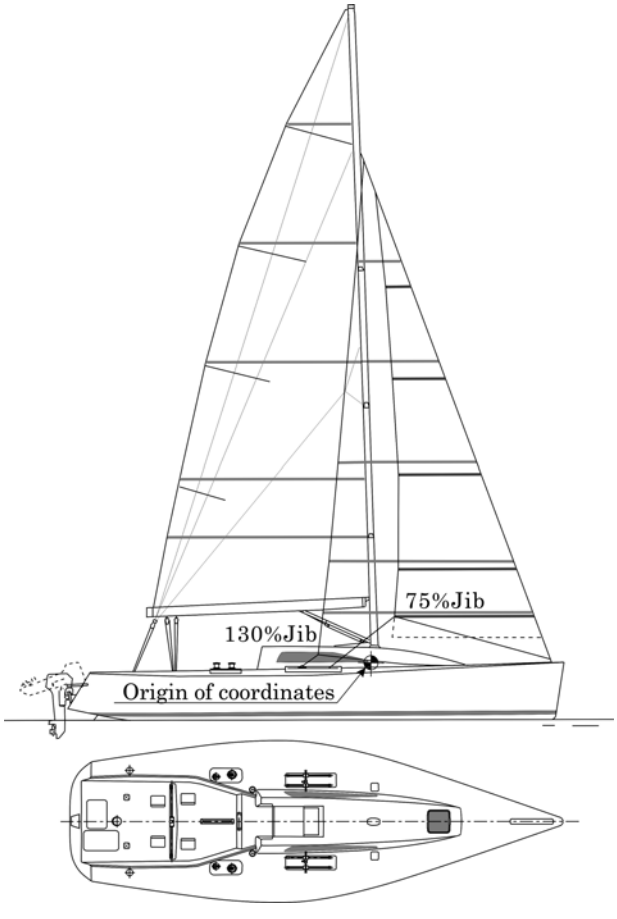

Fig. 1 Sail plan of *Fujin* with 130% jib and 75% jib

MEASUREMENTS OF FULL-SCALE SAIL PERFORMANCE AND SAIL SHAPE

Sail Dynamometer Boat *Fujin*

The design of the *Fujin* is based on the YR-10.3m class, which is an IMS ocean racer designed by Yamaha Motor Co. Ltd. Although the hull was made using a mold of that class, the deck and interior of the boat were modified to install the dynamometer frame inside of the hull and deck.

Measurement System of Aerodynamic Performance

The sail dynamometer system is composed of a rigid aluminum frame and four load cells. The frame is separated structurally from the hull and connected with it by these load cells. Figure 2 shows general arrangement of the dynamometer frame. The load cells are numbered in the figure. Two of these are 1-component load cells and the others are 2-component. Hence, these load cells form a 6-component dynamometer system, and their outputs can be transformed to the forces and moments about the boat axes using a calibration matrix. All rig components such as mast, chain plates, winches, lead blocks, etc. are attached to the aluminum frame. The under deck portion of the mast is held by the frame, and other rig components are attached to the bases extended from the frame through the deck holes. The data acquisition system and calibration method for the *Fujin* were mentioned in the previous paper (Masuyama et al. 1997).

Measurement System of Sail Shape and Others

The sail shape was recorded using CCD cameras. The lower part of the mainsail was photographed using two cameras; CCD cameras A in Figure 3, which were located at the mast top and 50 cm transversely from both sides of the mast. The upper part of the mainsail was photographed using a portable video camera from below the boom. The lower part of the jib was photographed using two cameras,

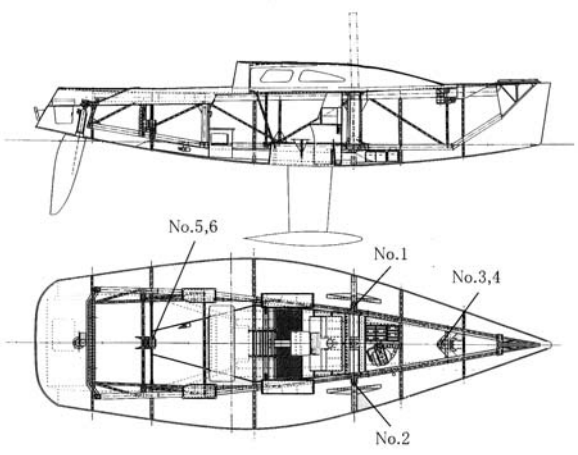

Fig. 2 General arrangement of dynamometer frame in *Fujin*

CCD cameras B in Figure 3, which were located at the "I" point of both sides of the mast. The upper part of the jib was photographed using a portable video camera from inside of the bow hatch. For measuring convenience, horizontal stripes were drawn on the mainsail and jib at the height of 10, 20, 40, 60 and 80% of each sail. The sail shape images are analyzed using the sail shape analyzing software, SSA-2D, developed by Armonicos Co. This software calculates the curvature of the sail section by marking several points of the sail stripe and the reference line on the PC display, and indicates the parameters such as chord length, maximum draft, maximum draft position, entry angle at the luff and exit angle at the leech as shown in Figure 4.

The twist angle of lower part of the sail measured from the upper camera is determined by taking the angle from the centerline of the boat as the reference line. On the other hand, the twist angle of upper part measured from lower camera might not be correct due to lack of a reference line. Therefore these twist angles were calibrated using the twist angle at 40% height which coincided with the measured angle from the upper camera. In the previous paper (Masuyama et al. 1997), the calibration of the twist angle of upper part was not sufficiently. Hence all of the measured sail shape data were reanalyzed for this report. From these data, three-dimensional coordinates of the sails are calculated by interpolation using spline curves.

The apparent wind speed (AWS) and apparent wind angle (AWA) are measured by an anemometer attached on the "Bow unit" as shown in Figure 3. This unit can rotate freely to keep vertical attitude even if the boat heels. The height of the anemometer coincides with the geometric center of effort (GCE) of the sail plan. The wind speed and wind angle sensors were calibrated by wind tunnel tests in advance.

The *Fujin* also has measuring instruments such as Optical Fiber Gyroscope (roll and pitch angles), Flux Gate Compass (heading angle), Differential type GPS receiver, speedometer and potentiometer for rudder angle. These data are recorded by an onboard computer simultaneously with data from the load cells.

The sea tests were performed inside of Nanao Bay in the Noto Peninsula. Approximate dimensions of the bay are 8 and 5 nautical miles from east to west and from north to south, respectively. The bay is surrounded by low hills, and mouth connecting the bay and the Japan Sea is narrow. Therefore, tidal currents are small, and wave heights are relatively low even though the wind can be strong.

Figure 5 shows the wind gradient with height above sea surface at this area. These wind gradients were measured using two anemometers set on the *Fujin* without sails. Filled circles indicate the data measured at the mast top (16.6m high from sea surface) and bow unit (6.5m high). Non-filled circles indicate the data measured attaching anemometers at the No.1 spreader (10.0m high) and No.3 spreader (4.5m high). Two circles connected by solid line or dotted line show the data measured simultaneously using two anemometers during 30 seconds. However the data of filled and non-filled circles were not measured at the same time. Therefore, the slope of solid or dotted lines indicates the wind gradient at each height respectively. In the figure, wind gradient curves indicating power-law profiles are also shown. The solid curves show 1/10 power and dotted curves 1/7 power. It can be seen that the wind gradient of this area is not so significant. From this reason, the wind gradient was not taken into account for the numerical calculation. This means the apparent wind angle and speed are assumed to be constant in the vertical direction. The numerical calculations were performed using the wind angle and speed which were measured at the bow unit, i.e. the height of GCE of the sail plan.

The close-hauled tests were conducted at the apparent wind angle (AWA) range of 20 degrees to 40 degrees, and the apparent wind speed (AWS) range of 5m/s to 11m/s. A person steered the boat to weather carefully. Variations of sail performance were measured with the change of AWA, draft of mainsail and twist of mainsail. Figure 3 shows a sea test condition in light wind with 130% jib.

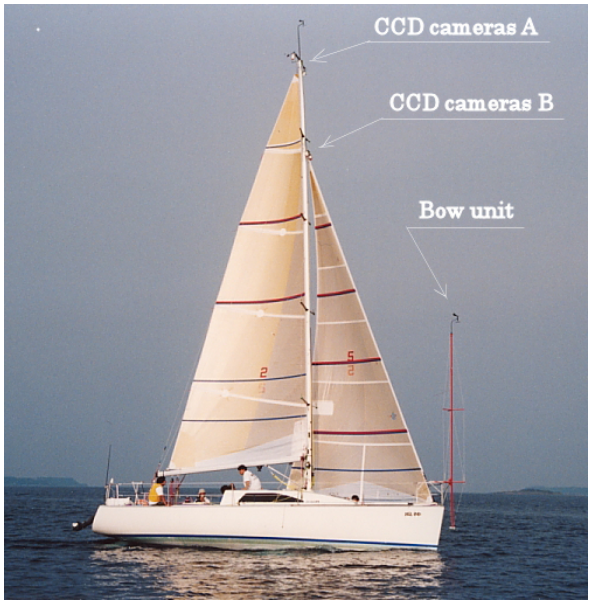

Fig. 3 Sea test condition in light wind with 130% jib

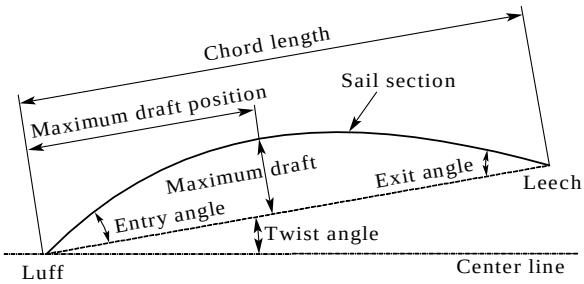

Fig. 4 Measured sail shape parameters

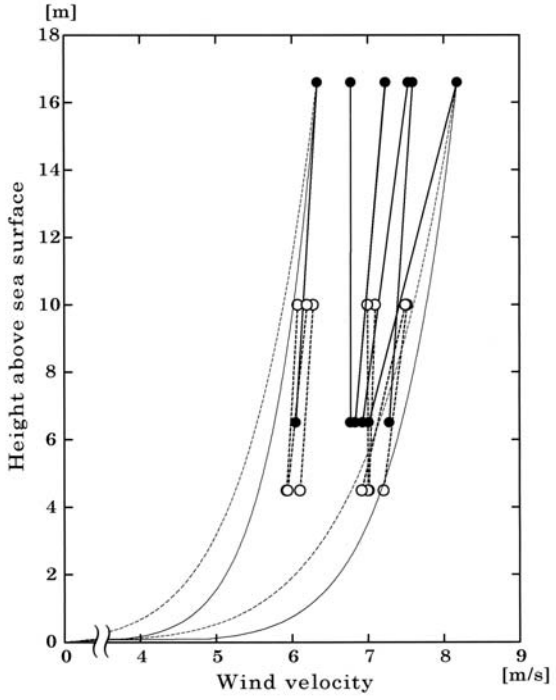

Fig.5 Wind gradient at sea test area

NUMERICAL CALCULATION METHOD

Vortex Lattice Method

As a potential flow calculation, a vortex lattice method was employed to compare with the results of a RANS-based CFD calculation. The sail surface is divided into rectangular panels, and a horseshoe bound vortex is placed on each panel at a distance of 1/4 panel length from the fore end of panel. Free wake vortices proceed downstream from the trailing edge of sail. Shapes and positions of wake vortices are determined so that the wake vortices are parallel to the local velocity field induced by the total vortex system.

A step-by-step procedure developed by Fukasawa (1993) is used to determine the strength of bound vortices and the location of wake vortices, and iterated until the calculated lift and drag forces converge. Strengths of bound vortices are determined so as to satisfy the boundary condition on the sail at the control points, which are placed on each panel at a distance of 1/4 panel length from the aft end of the panel. Wake vortices are shed from the trailing edge of the sail in each time step. Maintaining the vortex strength, the shed out vortex filament moves downstream at local field velocity in the direction of the field velocity vector, which is updated in every time step. Once all vortex strengths are determined, lift, induced drag, and moments acting on the sail are calculated. The detailed procedure was mentioned in the previous paper (Masuyama et al. 1997).

Since the vortex lattice method do not provide viscous drag, the viscous drag acting on the sails and rigging is calculated using drag coefficient C_{Dp}. The value of C_{Dp} was evaluated from the measured data in the previous paper and formulated for the upwind condition as follow:

$$C_{Dp} = 0.0026\ \gamma_A + 0.005 \qquad (2)$$

where γ_A is apparent wind angle in degrees.

The calculation was newly conducted for this report for all cases, because the measured sail shape data were reanalyzed for this report as above mentioned. In the calculations, each sail plane was divided into 200 panels; that is, 20 panels in the vertical direction and 10 panels in the horizontal direction. The mirror image of the sail was taken into account about the sea surface.

Multi-block RANS-Based CFD Method

The RANS-based CFD method used in the present study is FLOWPACK version 2005. The code has been developed by Tahara, particularly for CFD education and research, and design applications for ship hydrodynamics, aerodynamics, and fluid engineering. In the transition for design applications, complete multi-block domain decomposition, an automatic grid generation scheme, and a CAD interface are included. At present, FLOWPACK has a tight interface with both commercial and the author's in-house grid generators.

The numerical method of FLOWPACK solves the unsteady Reynolds-averaged Navier-Stokes and continuity equations for mean velocity and pressure. A zero or two-equation turbulence model (k-ε or k-ω) is used for turbulence flow calculation. The equations are transformed from Cartesian coordinates in the physical domain to numerically-generated, boundary-fitted, non-orthogonal, curvilinear coordinates in the computational domain. A partial transformation is used, i.e., coordinates but not velocity components. The equations are solved using a regular grid, finite-analytic spatial and first-order backward difference temporal discretization, and a PISO-type pressure algorithm.

The present RANS code was applied for predicting the flow field around series sail configurations obtained from the measurements. Figure 6 shows an overview of the computational grid for the present upwind sail system. An automatic gridding scheme developed by the author was used. The total number of grids is around a half million, and the number of multi blocks is 48. Input data for the present automatic gridding scheme are measured sail geometry, AWA and heel angle. In the computations, the Reynolds number, *Re*, is 5×10^6 (based on apparent wind speed and mast height), which is assumed to be in the full-scale condition.

In the following chapter, the series calculations were conducted for the sail configuration alone, i.e., without mast and rigging in order to apply the automatic gridding scheme. The bottom surface of computational grid was taken at the deck plane of the boat. The influence of turbulence models and mesh size, and existence of the mast on the calculation will be mentioned in the after next

chapters.

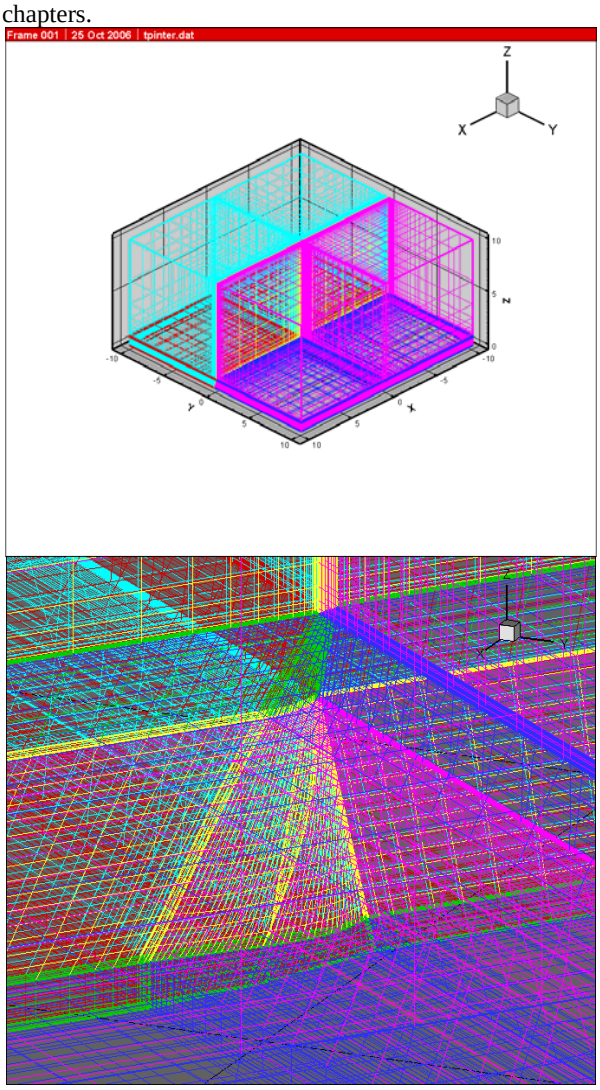

Fig. 6 Overview of computational grid. The present automatic gridding scheme was used. Total number of grids is around a half million, and the number of multi blocks is 48.

COMPARISON BETWEEN EXPRIMNTAL RESULTS AND CALCULATED RESULTS

In this chapter, we will show the comparison between experimental results and calculated results about following series:

(1) For the case of mainsail with 130% jib
  (a) Variation with apparent wind angle (AWA)
  (b) Variation with mainsail mean draft
  (c) Variation with mainsail twist angle
(2) For the case of mainsail with 75% jib
  (a) Variation with apparent wind angle (AWA)
(3) For the case of mainsail alone
  (a) Variation with mainsail twist angle.

For each series, at first, the sail coefficients such as C_L and C_D, C_X and C_Y, and coordinates of x_{CE} and z_{CE} are shown. Then, the calculated results of the sail surface pressure and streamlines by RANS-based CFD are shown for typical two cases in each series. Finally, the shapes and three-dimensional coordinates of the sails are tabulated for the cases, which coincide with the figured results by RANS-based CFD.

Mainsail with 130% Jib

Variation with Apparent Wind Angle

Figure 7 shows the performance variation of the configuration of mainsail and 130% jib with AWA. In the figure, (a) shows the variation of C_L and C_D, (b) shows C_X and C_Y, and (c) shows x_{CE} and z_{CE}, respectively. Filled marks indicate the experimental results and non-filled marks indicate the calculated results by VLM and RANS-based CFD. For the experimental results, both data of starboard tack and port tack are shown. There are some discrepancies between the data on each tack. During the experiments, efforts were made to remove this unsymmetrical performance. However, this was not compensated perfectly, and the boat speed actually differed on each tack. It can be concluded that there were slight unsymmetrical parts in the combination of the hull, keel, rudder and dynamometer frame.

The experimental data in this figure coincide with ones in the Figure 17 in the previous paper (Masuyama et al. 1997). However, some data points are eliminated due to lack of sail shape information or bad sail trimming. The numerical calculations were performed using these measured data. In order to avoid confusion interpreting the figure, the calculated results are indicated only for port tack. Therefore, the calculated and experimental points for port tack correspond to each other.

In the figure, the AWA ranges from 20.0 degrees to 38.2 degrees for port tack. The former is the closest angle to the wind to beating and the latter is in the range of close reaching condition, where the sail is trimmed in the power down mode. The experimental data slightly scattered because these data are composed of measurements under various sail trimming. The experimental value of C_L in the figure (a) varies from 0.91 to 1.61.

The calculated results of C_L by VLM show good agreement with the experiments at less than AWA range of 35 degrees. In the range of over 35 degrees, although the calculated results are lower than the measured, they clearly indicate the effect of power down mode. The results of C_L by RANS-based CFD are higher than the experiments in the range of 20 degrees to 30 degrees and lower in the range of over 30 degrees. In particular decreasing of C_L in the power down mode is significant. This will be discussed later with the calculated sail surface pressure and streamlines. The calculated results of C_D become a little bit larger than the experiments.

Figure (c) shows the coordinates of center of effort of

the sails. The x and z coordinates of geometric center of effort (GCE) are 0.63m backward and 4.80m upward from the origin, respectively, which are indicated by dotted lines in the figure. It is seen that the both experimental and calculated coordinates of x_{CE} exist at near x_{GCE} and move slightly backward with decreasing AWA. Unfortunately, the experimental values of z_{CE} fall into a relative wide region. This reason is considered as follow. The measured *Ks* moment contains a large amount of moment resulted from the mass of the dynamometer frame and rigging (659kg). This moment should be subtracted from the measured one by the calculation using measured heel angle. If there is slight error in the position of center of gravity of the dynamometer flame or in the measured heel angle, the error in the calculated moment becomes considerably large. Therefore, it is difficult to avoid containing a certain error in the measured value of z_{CE}. However, though the measured data are scattering, it can be seen that z_{CE} moves slightly upward with decreasing AWA. The tendencies of the movement of both x_{CE} and z_{CE} might be caused by the increment of forces acting on the aft and upper parts of the sails due to the tightening of main and jib sheets with decreasing AWA. The calculated results of z_{CE} by RANS-based CFD show the same tendency with the experiments. On the other hand, the results by VLM become considerably high. This might be caused by over estimation of force acting on the upper portion of the mainsail. In this area, since the jib is not overlapping, the flow separation may occur easily. However, VLM does not take the flow separation into account.

Figure 8 shows the calculated results of the sail surface pressure and streamlines by RANS-based CFD. The figure (1) indicates the case of experimental ID 96092335 (AWA= 30.5deg.), and (2) indicates 96080248 (AWA= 37.3deg.). These figure numbers coincide with ones described at the top of figure 7. In the figure 8, left and right columns correspond to the port and starboard sides, i.e., pressure and suction sides, respectively. In the case of (1), although slight flow separation on the suction side of mainsail is seen, the streamlines of both sides run smoothly. On the other hand, in the case of (2), considerable flow separation is occurring in particular on the suction side of jib. This is main reason of decreasing of calculated C_L value

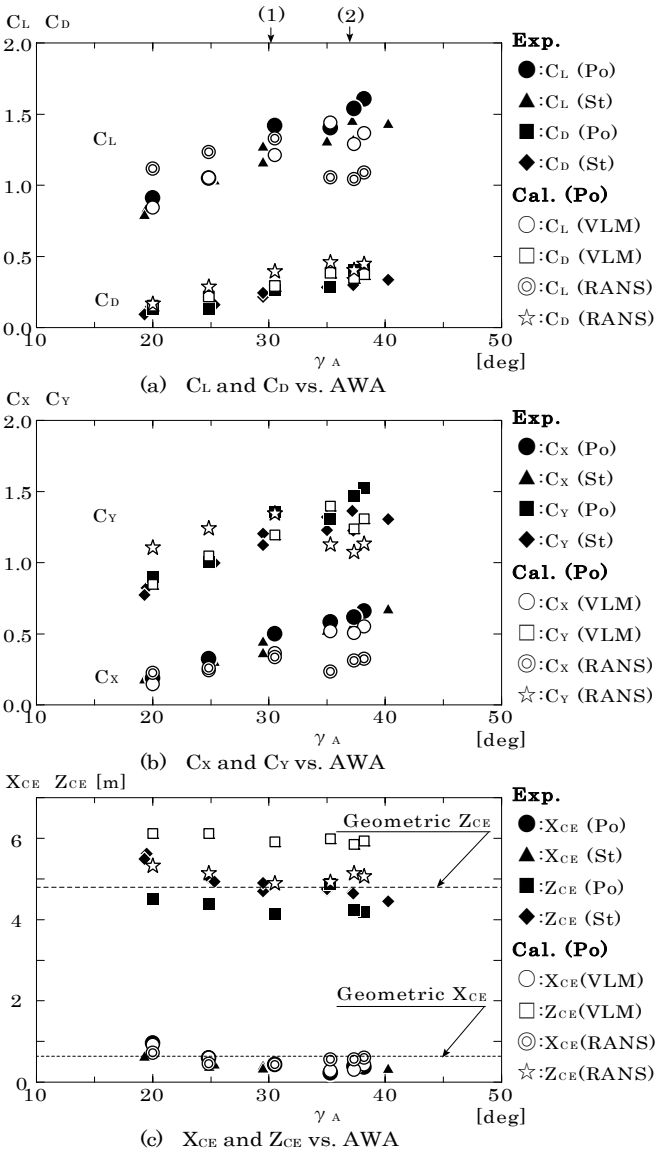

Fig.7 Performance variation with apparent wind angle (AWA) for mainsail and 130% jib

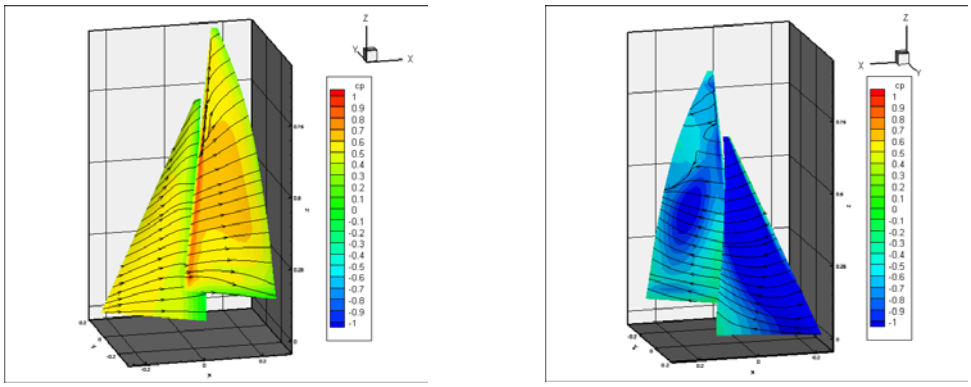

Fig. 8 (1) Comparison of surface pressure and streamlines obtained by RANS-based CFD at experimental ID 96092335 (AWA=30.5 deg.)

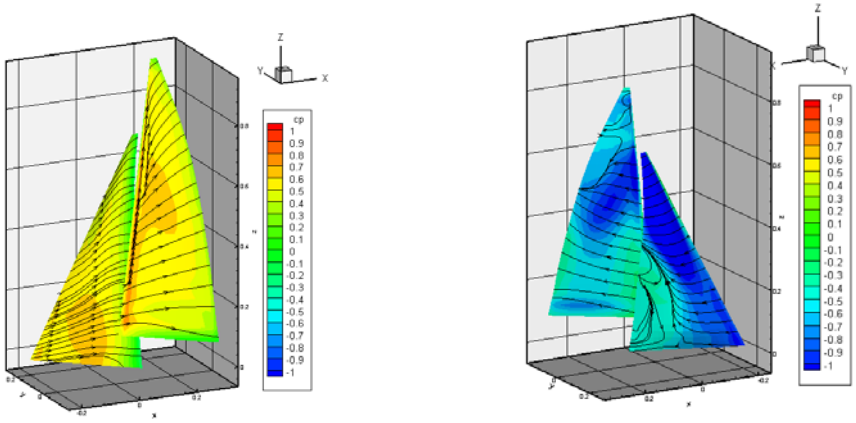

Fig. 8 (2) Comparison of surface pressure and streamlines obtained by RANS-based CFD at experimental ID 96080248 (AWA=37.3 deg.)

Table 3 Sail shapes, measured experimental data and three-dimensional coordinates of the sails for the cases of (1) 96092335 and (2) 96080248

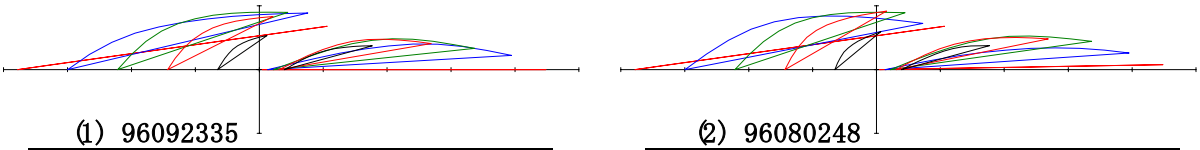

(1) 96092335

AWA[ ]	TWIST[ ]	DRAFT[%]	AWS[m/s]	HEEL[ ]	VB[kt]
-30.50	15.50	8.59	6.81	14.32	5.18
CL	CD	CX	CY	XCE[m]	ZCE[m]
1.418	0.260	0.498	1.354	0.433	4.138

%of height	130%Jib			Mainsail		
	x	y	z	x	y	z
	-3.780	0.000	0.000	0.046	0.000	1.320
	-2.812	0.136	0.000	0.934	0.000	1.320
0	-1.843	0.272	0.000	1.822	0.000	1.320
%	-0.875	0.408	0.000	2.710	0.000	1.320
	0.094	0.544	0.000	3.598	0.000	1.320
	1.062	0.681	0.000	4.486	0.000	1.320
	-2.998	0.000	2.140	0.133	0.000	3.820
	-2.305	0.429	2.140	0.888	0.176	3.820
20	-1.568	0.667	2.140	1.645	0.322	3.820
%	-0.805	0.795	2.140	2.406	0.400	3.820
	-0.027	0.861	2.140	3.173	0.363	3.820
	0.760	0.886	2.140	3.947	0.222	3.820
	-2.215	0.000	4.280	0.221	0.000	6.320
	-1.771	0.442	4.280	0.834	0.227	6.320
40	-1.272	0.719	4.280	1.452	0.405	6.320
%	-0.723	0.850	4.280	2.081	0.483	6.320
	-0.145	0.898	4.280	2.722	0.442	6.320
	0.448	0.898	4.280	3.371	0.331	6.320
	-1.433	0.000	6.420	0.308	0.000	8.820
	-1.186	0.332	6.420	0.761	0.218	8.820
60	-0.893	0.570	6.420	1.222	0.389	8.820
%	-0.552	0.715	6.420	1.699	0.470	8.820
	-0.176	0.790	6.420	2.191	0.462	8.820
	0.217	0.832	6.420	2.691	0.410	8.820
	-0.650	0.000	8.560	0.396	0.000	11.320
	-0.541	0.172	8.560	0.651	0.144	11.320
80	-0.414	0.318	8.560	0.914	0.261	11.320
%	-0.255	0.419	8.560	1.190	0.330	11.320
	-0.073	0.486	8.560	1.476	0.362	11.320
	0.122	0.535	8.560	1.768	0.374	11.320
	0.132	0.000	10.700	0.483	0.000	13.820
	0.144	0.016	10.700	0.511	0.012	13.820
100	0.159	0.030	10.700	0.538	0.023	13.820
%	0.173	0.044	10.700	0.567	0.033	13.820
	0.189	0.056	10.700	0.595	0.042	13.820
	0.207	0.066	10.700	0.624	0.051	13.820

(2) 96080248

AWA[ ]	TWIST[ ]	DRAFT[%]	AWS[m/s]	HEEL[ ]	VB[kt]
-37.33	14.50	7.23	7.52	21.32	5.87
CL	CD	CX	CY	XCE[m]	ZCE[m]
1.539	0.402	0.615	1.466	0.386	4.230

%of height	130%Jib			Mainsail		
	x	y	z	x	y	z
	-3.780	0.000	0.000	0.046	0.000	1.320
	-2.812	0.136	0.000	0.934	0.015	1.320
0	-1.843	0.272	0.000	1.822	0.031	1.320
%	-0.875	0.408	0.000	2.710	0.046	1.320
	0.094	0.544	0.000	3.597	0.062	1.320
	1.062	0.681	0.000	4.485	0.077	1.320
	-2.998	0.000	2.140	0.133	0.000	3.820
	-2.314	0.461	2.140	0.891	0.150	3.820
20	-1.597	0.750	2.140	1.651	0.267	3.820
%	-0.841	0.840	2.140	2.414	0.331	3.820
	-0.062	0.810	2.140	3.182	0.333	3.820
	0.728	0.724	2.140	3.954	0.262	3.820
	-2.215	0.000	4.280	0.221	0.000	6.320
	-1.769	0.437	4.280	0.829	0.239	6.320
40	-1.274	0.729	4.280	1.445	0.423	6.320
%	-0.726	0.863	4.280	2.074	0.520	6.320
	-0.145	0.899	4.280	2.717	0.511	6.320
	0.450	0.892	4.280	3.368	0.442	6.320
	-1.433	0.000	6.420	0.308	0.000	8.820
	-1.218	0.362	6.420	0.757	0.230	8.820
60	-0.940	0.615	6.420	1.218	0.397	8.820
%	-0.601	0.763	6.420	1.697	0.482	8.820
	-0.230	0.854	6.420	2.187	0.504	8.820
	0.157	0.918	6.420	2.687	0.481	8.820
	-0.650	0.000	8.560	0.396	0.000	11.320
	-0.565	0.191	8.560	0.656	0.128	11.320
80	-0.445	0.339	8.560	0.921	0.241	11.320
%	-0.289	0.444	8.560	1.193	0.327	11.320
	-0.113	0.527	8.560	1.478	0.368	11.320
	0.071	0.597	8.560	1.771	0.377	11.320
	0.132	0.000	10.700	0.483	0.000	13.820
	0.142	0.018	10.700	0.511	0.011	13.820
100	0.154	0.034	10.700	0.539	0.022	13.820
%	0.167	0.049	10.700	0.567	0.032	13.820
	0.181	0.064	10.700	0.596	0.041	13.820
	0.196	0.077	10.700	0.625	0.049	13.820

at (2) in the figure (a). Further consideration of the results of CFD will be mentioned in the following chapter.

Table 3 shows the shapes and three-dimensional coordinates of the sails. The numbered (1) and (2) tables correspond to the cases of experimental ID 96092335 and 96080248, respectively. These also correspond to the calculated results shown in figure 8. The figures described above the tables show the sail section profiles at 0, 20, 40, 60 and 80% of the sail height. These three-dimensional coordinates in meter unit are listed in the tables including 100% height section data. The origin of the coordinates is mentioned in the chapter two and minus value in x coordinate means directing forward. In the four lines of top of the tables, the measured data at experiments are also shown, which are wind and sail trim conditions, the boat attitude and the sail performance coefficients.

Variation with Mainsail Mean Draft

Figure 9 shows the performance variation of the configuration of mainsail and 130% jib with mainsail mean draft. The notations of all figures in this chapter are same as the former section. The experimental data in this figure coincide with ones in the Figure 18 in the previous paper. Some data points are eliminated by the same reason with the former section.

The mainsail draft was changed by varying the tensions of the back stay and check stay, and the position of the mainsail outhaul. The twist of the mainsail was controlled to keep the exit angle of the top batten parallel with boom angle by varying the main sheet tension. The experiment was performed keeping AWA as 30 degrees and twist angle as around 16 degrees. The jib shape was fixed during varying the mainsail draft. The mean draft is defined as the average of maximum draft of four sections of the mainsail from 20% to 80% heights.

In the figure, the mean draft ranges from 6.6% to 13.1% for port tack. By varying of 6.5% in mean draft, the value of C_X in figure (b) changes from 0.47 to 0.59 (21%), and C_Y from 1.26 to 1.49 (18%). It ca be seen that the maximum C_X (i.e. thrust) point exists at around 10 to 12% of mean draft. Although the calculated results of C_X and C_Y indicate slight lower values than the measured, the tendency

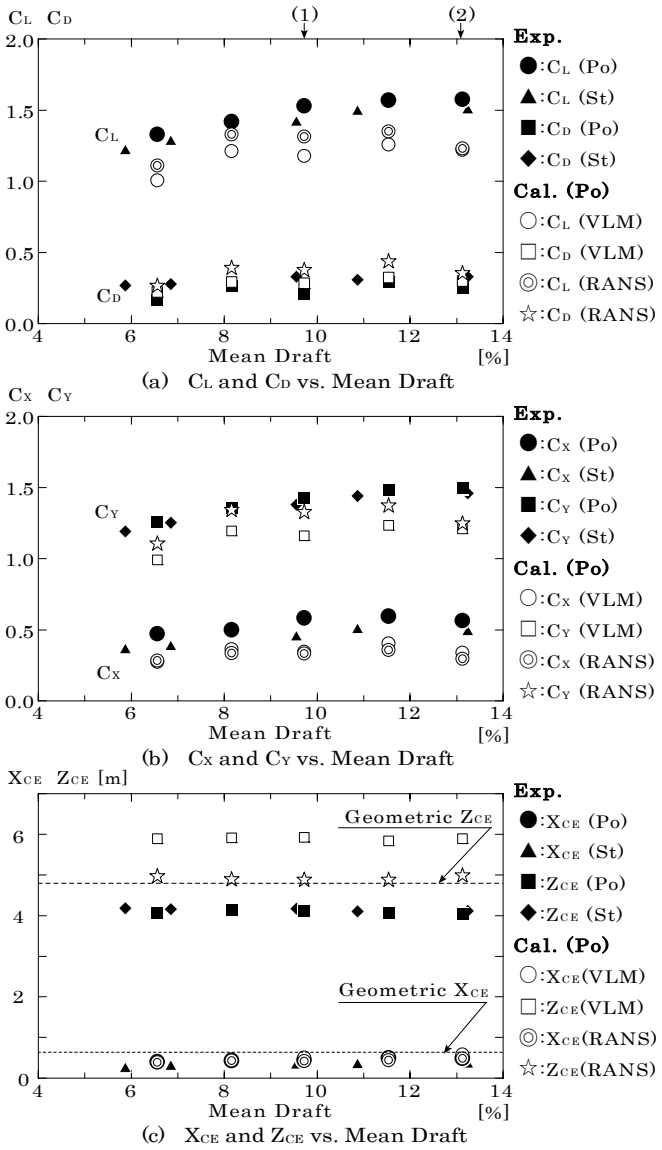

Fig.9 Performance variation with mainsail mean draft for mainsail and 130% jib

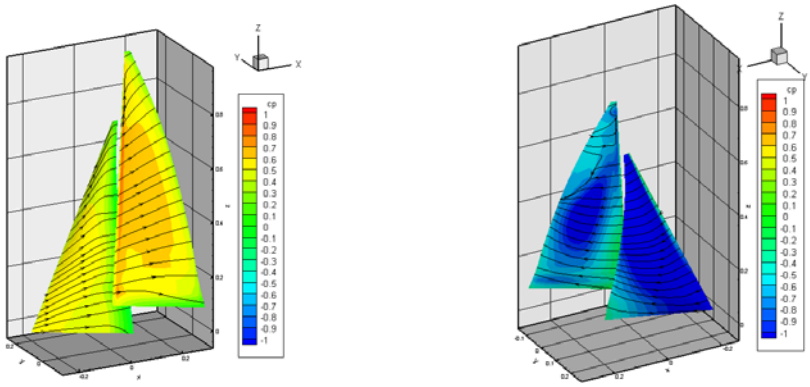

Fig. 10 (1) Comparison of surface pressure and streamlines obtained by RANS-based CFD at experimental ID 96092336 (mean draft= 9.7%)

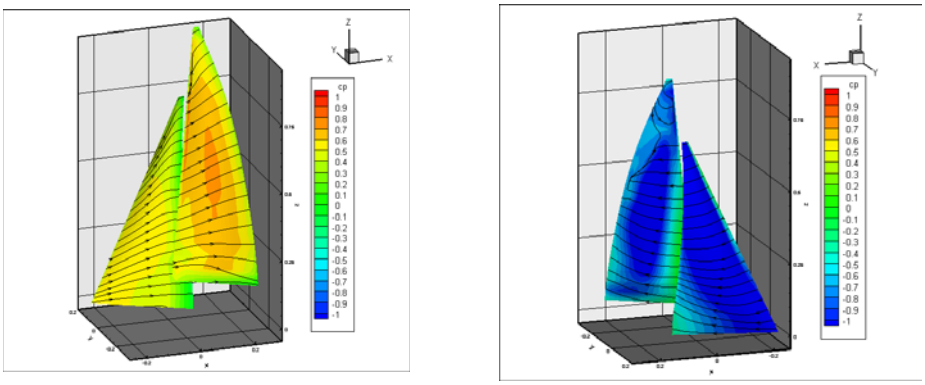

Fig. 10 (2) Comparison of surface pressure and streamlines obtained by RANS-based CFD at experimental ID 9609233A (mean draft= 13.1%)

Table 4 Sail shapes, measured experimental data and three-dimensional coordinates of the sails for the cases of (1) 96092336 and (2) 9609233A

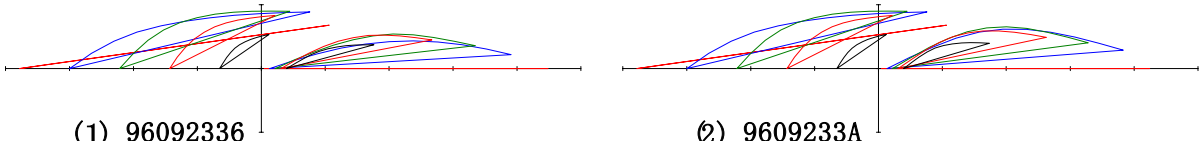

(1) 96092336

AWA[ ]	TWIST[ ]	DRAFT[%]	AWS[m/s]	HEEL[ ]	VB[kt]
-30.00	15.50	9.72	7.37	18.24	5.42
CL	CD	CX	CY	XCE[m]	ZCE[m]
1.529	0.210	0.583	1.429	0.445	4.120

%of heit	130%Jib			Mainsail		
	x	y	z	x	y	z
	-3.780	0.000	0.000	0.046	0.000	1.320
	-2.812	0.136	0.000	0.934	0.000	1.320
0	-1.843	0.272	0.000	1.822	0.000	1.320
%	-0.875	0.408	0.000	2.710	0.000	1.320
	0.094	0.544	0.000	3.598	0.000	1.320
	1.062	0.681	0.000	4.486	0.000	1.320
	-2.998	0.000	2.140	0.133	0.000	3.820
	-2.305	0.429	2.140	0.878	0.232	3.820
20	-1.568	0.667	2.140	1.626	0.385	3.820
%	-0.805	0.795	2.140	2.381	0.433	3.820
	-0.027	0.861	2.140	3.141	0.373	3.820
	0.760	0.886	2.140	3.908	0.216	3.820
	-2.215	0.000	4.280	0.221	0.000	6.320
	-1.771	0.442	4.280	0.825	0.259	6.320
40	-1.272	0.719	4.280	1.437	0.451	6.320
%	-0.723	0.850	4.280	2.060	0.541	6.320
	-0.145	0.898	4.280	2.700	0.488	6.320
	0.448	0.898	4.280	3.348	0.356	6.320
	-1.433	0.000	6.420	0.308	0.000	8.820
	-1.186	0.332	6.420	0.751	0.243	8.820
60	-0.893	0.570	6.420	1.205	0.427	8.820
%	-0.552	0.715	6.420	1.677	0.518	8.820
	-0.176	0.790	6.420	2.168	0.509	8.820
	0.217	0.832	6.420	2.669	0.449	8.820
	-0.650	0.000	8.560	0.396	0.000	11.320
	-0.541	0.172	8.560	0.649	0.149	11.320
80	-0.414	0.318	8.560	0.910	0.270	11.320
%	-0.255	0.419	8.560	1.185	0.340	11.320
	-0.073	0.486	8.560	1.471	0.368	11.320
	0.122	0.535	8.560	1.764	0.373	11.320
	0.132	0.000	10.700	0.483	0.000	13.820
	0.144	0.016	10.700	0.511	0.012	13.820
100	0.159	0.030	10.700	0.538	0.023	13.820
%	0.173	0.044	10.700	0.567	0.033	13.820
	0.189	0.056	10.700	0.595	0.042	13.820
	0.207	0.066	10.700	0.624	0.051	13.820

(2) 9609233A

AWA[ ]	TWIST[ ]	DRAFT[%]	AWS[m/s]	HEEL[ ]	VB[kt]
-29.25	16.63	13.12	6.94	16.63	5.35
CL	CD	CX	CY	XCE[m]	ZCE[m]
1.577	0.247	0.564	1.493	0.490	4.032

%of heit	130%Jib			Mainsail		
	x	y	z	x	y	z
	-3.780	0.000	0.000	0.046	0.000	1.320
	-2.812	0.136	0.000	0.886	0.000	1.320
0	-1.843	0.272	0.000	1.726	0.000	1.320
%	-0.875	0.408	0.000	2.566	0.000	1.320
	0.094	0.544	0.000	3.406	0.000	1.320
	1.062	0.681	0.000	4.246	0.000	1.320
	-2.998	0.000	2.140	0.133	0.000	3.820
	-2.305	0.429	2.140	0.851	0.336	3.820
20	-1.568	0.667	2.140	1.577	0.572	3.820
%	-0.805	0.795	2.140	2.318	0.614	3.820
	-0.027	0.861	2.140	3.071	0.493	3.820
	0.760	0.886	2.140	3.831	0.286	3.820
	-2.215	0.000	4.280	0.221	0.000	6.320
	-1.771	0.442	4.280	0.800	0.331	6.320
40	-1.272	0.719	4.280	1.391	0.576	6.320
%	-0.723	0.850	4.280	2.004	0.653	6.320
	-0.145	0.898	4.280	2.638	0.570	6.320
	0.448	0.898	4.280	3.283	0.403	6.320
	-1.433	0.000	6.420	0.308	0.000	8.820
	-1.186	0.332	6.420	0.733	0.284	8.820
60	-0.893	0.570	6.420	1.171	0.501	8.820
%	-0.552	0.715	6.420	1.637	0.589	8.820
	-0.176	0.790	6.420	2.126	0.568	8.820
	0.217	0.832	6.420	2.628	0.490	8.820
	-0.650	0.000	8.560	0.396	0.000	11.320
	-0.541	0.172	8.560	0.634	0.180	11.320
80	-0.414	0.318	8.560	0.885	0.319	11.320
%	-0.255	0.419	8.560	1.156	0.386	11.320
	-0.073	0.486	8.560	1.442	0.404	11.320
	0.122	0.535	8.560	1.736	0.395	11.320
	0.132	0.000	10.700	0.483	0.000	13.820
	0.144	0.016	10.700	0.511	0.012	13.820
100	0.159	0.030	10.700	0.538	0.024	13.820
%	0.173	0.044	10.700	0.566	0.035	13.820
	0.189	0.056	10.700	0.595	0.044	13.820
	0.207	0.066	10.700	0.623	0.054	13.820

of change with the mean draft is well captured.

Figure 10 shows the calculated results of RANS-based CFD. The figure (1) indicates ID 96092336 (mean draft= 9.7%), and (2) indicates 9609233A (mean draft= 13.1%). It is seen that the high pressure area in the pressure side of mainsail of (2) locates afterward due to the larger draft than the case of (1). This causes decreasing of the thrust force of mainsail and resulted low value of C_X in figure (b). Table 4 shows the shapes and three-dimensional coordinates of the sails for the cases of (1) and (2), which correspond to the calculated results shown in figure 10.

Variation with Mainsail Twist Angle

Figure 11 shows the performance variation of the configuration of mainsail and 130% jib with mainsail twist angle. The mainsail twist was changed by varying the main sheet tension. The boom angle was kept to be parallel with the boat centerline by moving main sheet traveler. The experiment was performed keeping AWA as 30 degrees and mean draft as around 10%. The jib shape was fixed during varying the mainsail twist. The twist angle is defined as the angle between boom line and section chord line at 80% height.

In the figure, the twist angle ranges from 4.5 degrees to 24.9 degrees for port tack. By varying of 20.4 degrees in twist angle, the value of C_X in figure (b) changes from 0.35 to 0.41 (17%), and C_Y from 1.17 to 1.40 (20%). It ca be seen that the maximum C_X (i.e. thrust) point exists at around 15 degrees of twist angle. The considerable decreasing of C_Y with increasing of twist angle is also worth notice. In this case, the calculated results of C_X and C_Y, and C_L and C_D correspond to the measured values very well.

Figure 12 shows the calculated results of RANS-based CFD. The figure (1) indicates ID 97072213 (twist angle= 8.2 deg.), and (2) indicates 97072218 (twist angle= 24.1 deg.). It is seen that the streamlines of upper part of the suction side of mainsail of (1) show considerable flow separation. This is caused by large attack angle at the upper part due to small twist angle. On the other hand in (2), there is a low negative pressure area at the luff of suction side of mainsail due to small attack angle. This causes considerable decreasing of the value of C_X in figure (b). Table 5 shows

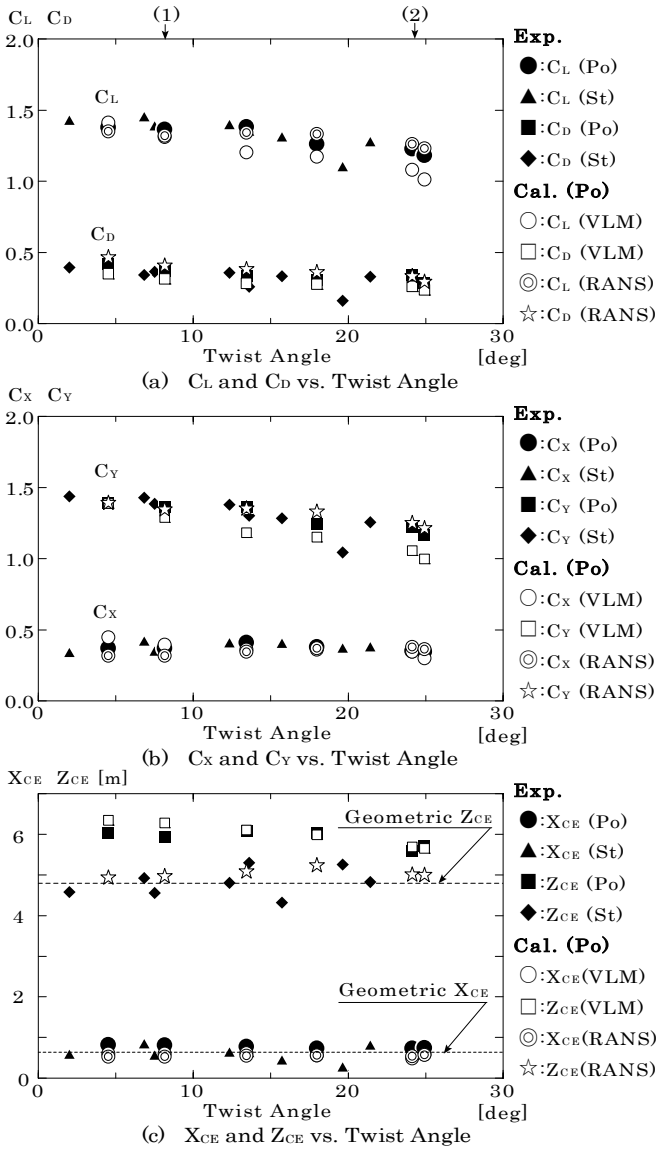

Fig.11 Performance variation with mainsail twist angle for mainsail and 130% jib

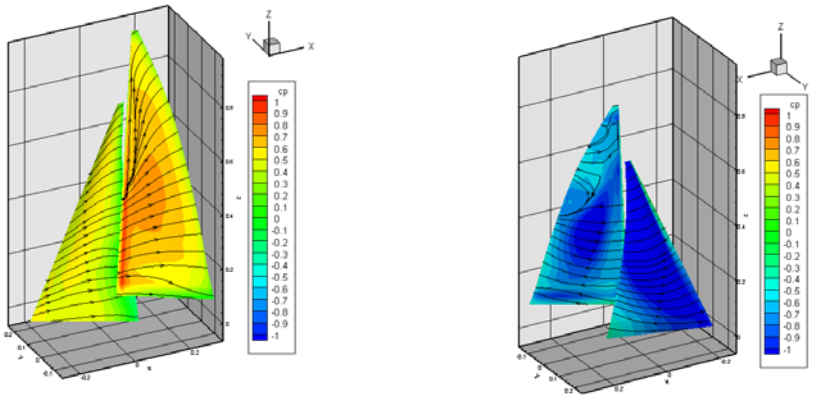

Fig. 12 (1) Comparison of surface pressure and streamlines obtained by RANS-based CFD at experimental ID 97072213 (twist angle= 8.2 deg.)

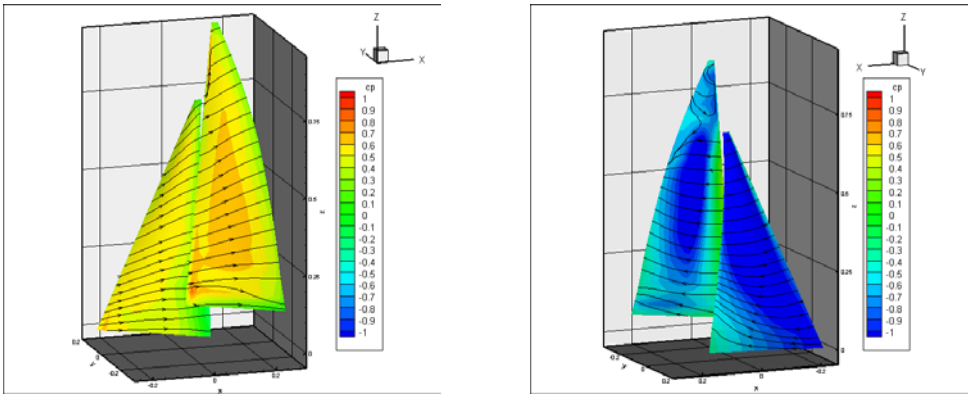

Fig. 12 (2) Comparison of surface pressure and streamlines obtained by RANS-based CFD at experimental ID 97072218 (twist angle= 24.1 deg.)

Table 5 Sail shapes, measured experimental data and three-dimensional coordinates of the sails for the cases of (1) 97072213 and (2) 97072218

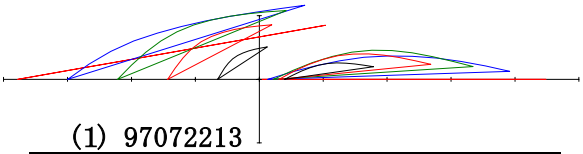

(1) 97072213

	AWA[°]	TWIST[°]	DRAFT[%]	AWS[m/s]	HEEL[°]	VB[kt]
	-30.42	8.16	10.48	7.29	16.91	5.13
	CL	CD	CX	CY	XCE[m]	ZCE[m]
	1.363	0.373	0.369	1.365	0.808	5.938

%of height	130%Jib			Mainsail		
	x	y	z	x	y	z
	-3.780	0.000	0.000	0.046	0.000	1.320
	-2.817	0.170	0.000	0.934	0.000	1.320
0	-1.854	0.340	0.000	1.822	0.000	1.320
%	-0.891	0.509	0.000	2.710	0.000	1.320
	0.073	0.679	0.000	3.598	0.000	1.320
	1.036	0.849	0.000	4.486	0.000	1.320
	-2.998	0.000	2.140	0.133	0.000	3.820
	-2.320	0.440	2.140	0.884	0.214	3.820
20	-1.595	0.727	2.140	1.638	0.345	3.820
%	-0.839	0.917	2.140	2.395	0.362	3.820
	-0.067	1.055	2.140	3.156	0.283	3.820
	0.714	1.165	2.140	3.919	0.125	3.820
	-2.215	0.000	4.280	0.221	0.000	6.320
	-1.774	0.427	4.280	0.832	0.263	6.320
40	-1.289	0.746	4.280	1.449	0.427	6.320
%	-0.750	0.933	4.280	2.076	0.452	6.320
	-0.174	1.031	4.280	2.710	0.358	6.320
	0.421	1.082	4.280	3.348	0.199	6.320
	-1.433	0.000	6.420	0.308	0.000	8.820
	-1.193	0.336	6.420	0.766	0.231	8.820
60	-0.911	0.590	6.420	1.232	0.372	8.820
%	-0.573	0.737	6.420	1.710	0.399	8.820
	-0.199	0.816	6.420	2.196	0.340	8.820
	0.196	0.855	6.420	2.687	0.235	8.820
	-0.650	0.000	8.560	0.396	0.000	11.320
	-0.543	0.176	8.560	0.662	0.130	11.320
80	-0.416	0.322	8.560	0.932	0.224	11.320
%	-0.255	0.414	8.560	1.212	0.259	11.320
	-0.070	0.472	8.560	1.499	0.241	11.320
	0.128	0.510	8.560	1.789	0.197	11.320
	0.132	0.000	10.700	0.483	0.000	13.820
	0.145	0.016	10.700	0.512	0.007	13.820
100	0.161	0.028	10.700	0.541	0.014	13.820
%	0.177	0.041	10.700	0.571	0.019	13.820
	0.193	0.052	10.700	0.601	0.023	13.820
	0.212	0.060	10.700	0.630	0.027	13.820

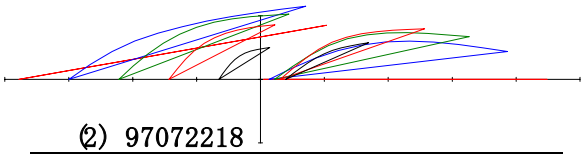

(2) 97072218

	AWA[°]	TWIST[°]	DRAFT[%]	AWS[m/s]	HEEL[°]	VB[kt]
	-31.67	24.13	10.55	7.29	13.44	5.25
	CL	CD	CX	CY	XCE[m]	ZCE[m]
	1.227	0.344	0.352	1.225	0.733	5.586

%of height	130%Jib			Mainsail		
	x	y	z	x	y	z
	-3.780	0.000	0.000	0.046	0.000	1.320
	-2.817	0.170	0.000	0.934	0.000	1.320
0	-1.854	0.340	0.000	1.822	0.000	1.320
%	-0.891	0.509	0.000	2.710	0.000	1.320
	0.073	0.679	0.000	3.598	0.000	1.320
	1.036	0.849	0.000	4.486	0.000	1.320
	-2.998	0.000	2.140	0.133	0.000	3.820
	-2.321	0.439	2.140	0.852	0.328	3.820
20	-1.598	0.728	2.140	1.584	0.539	3.820
%	-0.844	0.914	2.140	2.334	0.601	3.820
	-0.073	1.048	2.140	3.097	0.548	3.820
	0.708	1.151	2.140	3.866	0.437	3.820
	-2.215	0.000	4.280	0.221	0.000	6.320
	-1.760	0.403	4.280	0.777	0.378	6.320
40	-1.266	0.707	4.280	1.358	0.638	6.320
%	-0.729	0.898	4.280	1.977	0.730	6.320
	-0.151	0.985	4.280	2.617	0.721	6.320
	0.444	1.025	4.280	3.268	0.669	6.320
	-1.433	0.000	6.420	0.308	0.000	8.820
	-1.173	0.313	6.420	0.701	0.328	8.820
60	-0.883	0.565	6.420	1.119	0.582	8.820
%	-0.544	0.724	6.420	1.580	0.716	8.820
	-0.168	0.811	6.420	2.068	0.771	8.820
	0.229	0.858	6.420	2.568	0.794	8.820
	-0.650	0.000	8.560	0.396	0.000	11.320
	-0.533	0.166	8.560	0.627	0.179	11.320
80	-0.401	0.310	8.560	0.868	0.335	11.320
%	-0.243	0.411	8.560	1.127	0.453	11.320
	-0.056	0.467	8.560	1.406	0.525	11.320
	0.146	0.500	8.560	1.694	0.576	11.320
	0.132	0.000	10.700	0.483	0.000	13.820
	0.145	0.016	10.700	0.509	0.015	13.820
100	0.161	0.028	10.700	0.535	0.031	13.820
%	0.177	0.040	10.700	0.561	0.045	13.820
	0.193	0.052	10.700	0.588	0.057	13.820
	0.212	0.060	10.700	0.615	0.070	13.820

the shapes and three-dimensional coordinates of the sails for the cases of (1) and (2), which correspond to the calculated results shown in figure 12.

Mainsail with 75% Jib

Variation with Apparent Wind Angle

Figure 13 shows the performance variation of the configuration of mainsail and 75% jib with AWA. Unfortunately, the longitudinal position of the jib rail track was located a little bit afterward than the suitable leading point of 75% jib. Hence the upper part of the sail was not trimmed sufficiently. This caused the gentle variation of C_L in figure (a) comparing with Figure 7(a). It should be noted that the sail area for the non-dimensionalization in this case is 46.9m^2, which is 79% of the case of mainsail with 130% jib. Although the results of C_L by VLM increase monotonously with AWA, the results by RANS-based CFD show good agreement with the experiment. However, the calculated C_D at AWA= 29.8 deg. (ID 98110108) is considerably high, and that is clearly overestimated. This discrepancy is likely due to an extreme suction-side flow separation predicted in computational results. A possible reason to this issue is insufficient grid resolution and inadequate representation of sail geometry in computational grid especially near the leading edge. RANS-based CFD may tend to be sensitive to accuracy in grid, and over-predict flow separation especially for a large AWA. More investigation on this issue will be continued to identify the cause and solutions. In the figure (c), the x and z coordinates of GCE for this configuration are 0.85m backward and 5.14m upward from the origin, respectively. The experimental data are close to these values.

Figure 14 shows the calculated results of RANS-based CFD. The figure (1) indicates ID 98110105 (AWA= 20.5 deg.), and (2) indicates 9811032A (AWA= 35.2 deg.). In both cases, it is seen that the streamlines at the upper part of the pressure side of jib show considerable flow separation. This is caused by the small attack angle at the upper part due to unsuitable jib sheet leading. Table 6 shows the shapes and three-dimensional coordinates of the sails for the cases of (1) and (2), which correspond to the calculated results

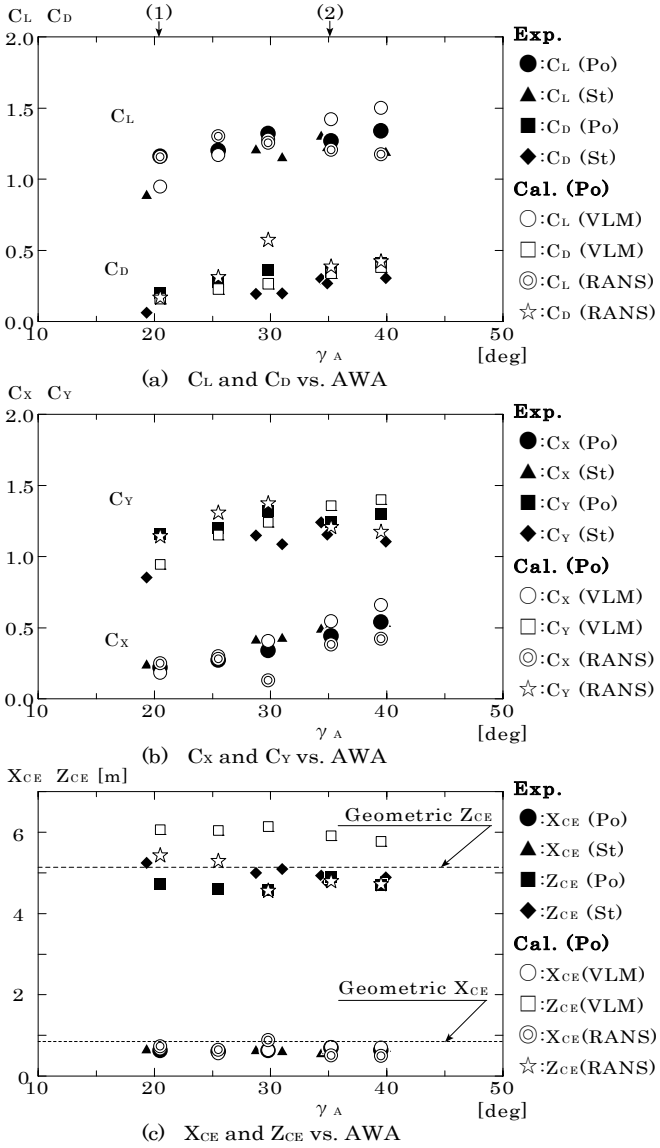

Fig.13 Performance variation with apparent wind angle (AWA) for mainsail and 75% jib

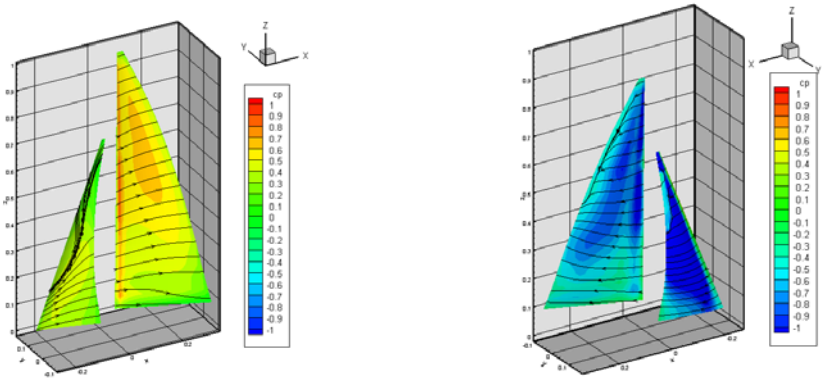

Fig. 14 (1) Comparison of surface pressure and streamlines obtained by RANS-based CFD at experimental ID 98110105 (AWA= 20.5 deg.)

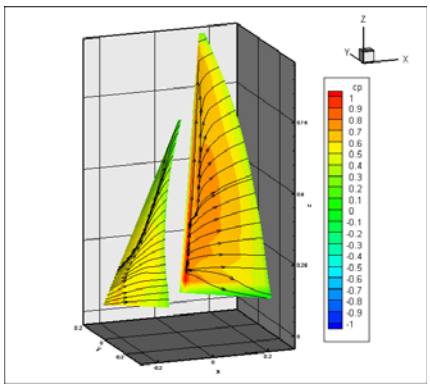

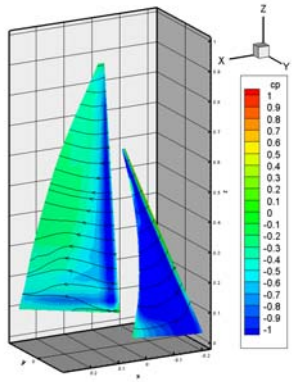

Fig. 14 (2) Comparison of surface pressure and streamlines obtained by RANS-based CFD at experimental ID 9811032A (AWA= 35.2 deg.)

Table 6 Sail shapes, measured experimental data and three-dimensional coordinates of the sails for the cases of (1) 98110105 and (2) 9811032A

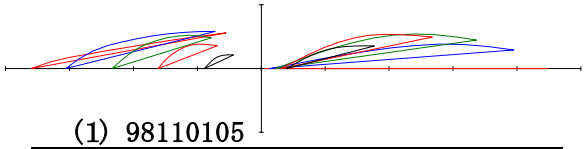

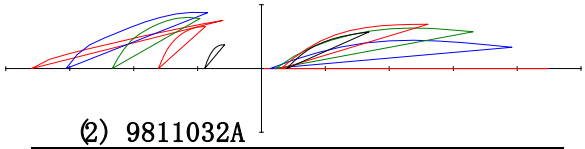

(1) 98110105

AWA[ ]	TWIST[ ]	DRAFT[%]	AWS[m/s]	HEEL[ ]	VB[kt]
-20.50	14.53	7.93	8.52	11.24	4.83
CL	CD	CX	CY	XCE[m]	ZCE[m]
1.164	0.199	0.220	1.161	0.623	4.738

%of heit	75%Jib			Mainsail		
	x	y	z	x	y	z
Jib	-3.599	0.000	0.495	0.046	0.000	1.32
5%	-3.001	0.173	0.495	0.934	0.000	1.32
	-2.392	0.282	0.495	1.822	0.000	1.32
Main	-1.780	0.384	0.495	2.710	0.000	1.32
0%	-1.168	0.476	0.495	3.598	0.000	1.32
	-0.553	0.557	0.495	4.486	0.000	1.32
	-3.057	0.000	1.980	0.133	0.000	3.820
	-2.630	0.274	1.980	0.890	0.142	3.820
20	-2.170	0.418	1.980	1.648	0.271	3.820
%	-1.697	0.511	1.980	2.409	0.361	3.820
	-1.215	0.567	1.980	3.175	0.375	3.820
	-0.723	0.581	1.980	3.949	0.289	3.820
	-2.335	0.000	3.960	0.221	0.000	6.320
	-2.065	0.228	3.960	0.831	0.223	6.320
40	-1.776	0.391	3.960	1.447	0.409	6.320
%	-1.464	0.481	3.960	2.073	0.524	6.320
	-1.136	0.520	3.960	2.714	0.531	6.320
	-0.783	0.479	3.960	3.368	0.448	6.320
	-1.612	0.000	5.940	0.308	0.000	8.820
	-1.464	0.167	5.940	0.755	0.226	8.820
60	-1.298	0.287	5.940	1.211	0.411	8.820
%	-1.115	0.365	5.940	1.683	0.519	8.820
	-0.908	0.380	5.940	2.175	0.532	8.820
	-0.687	0.358	5.940	2.677	0.495	8.820
	-0.890	0.000	7.920	0.396	0.000	11.320
	-0.816	0.080	7.920	0.652	0.143	11.320
80	-0.738	0.150	7.920	0.914	0.261	11.320
%	-0.648	0.196	7.920	1.189	0.330	11.320
	-0.546	0.213	7.920	1.476	0.353	11.320
	-0.435	0.212	7.920	1.769	0.353	11.320
	-0.167	0.000	9.900	0.483	0.000	13.820
	-0.152	0.014	9.900	0.511	0.010	13.820
100	-0.135	0.025	9.900	0.540	0.020	13.820
%	-0.118	0.036	9.900	0.568	0.029	13.820
	-0.101	0.045	9.900	0.597	0.036	13.820
	-0.081	0.052	9.900	0.626	0.044	13.820

(2) 9811032A

AWA[ ]	TWIST[ ]	DRAFT[%]	AWS[m/s]	HEEL[ ]	VB[kt]
-35.20	24.36	9.49	7.47	9.47	5.89
CL	CD	CX	CY	XCE[m]	ZCE[m]
1.267	0.355	0.441	1.240	0.695	4.904

%of heit	75%Jib			Mainsail		
	x	y	z	x	y	z
Jib	-3.599	0.000	0.495	0.046	0.000	1.32
5%	-3.020	0.231	0.495	0.934	0.000	1.32
	-2.420	0.377	0.495	1.822	0.000	1.32
Main	-1.817	0.514	0.495	2.710	0.000	1.32
0%	-1.212	0.641	0.495	3.598	0.000	1.32
	-0.604	0.756	0.495	4.486	0.000	1.32
	-3.057	0.000	1.980	0.133	0.000	3.820
	-2.691	0.370	1.980	0.875	0.248	3.820
20	-2.254	0.561	1.980	1.625	0.400	3.820
%	-1.810	0.733	1.980	2.384	0.442	3.820
	-1.345	0.853	1.980	3.151	0.406	3.820
	-0.842	0.876	1.980	3.920	0.331	3.820
	-2.335	0.000	3.960	0.221	0.000	6.320
	-2.148	0.310	3.960	0.798	0.338	6.320
40	-1.914	0.539	3.960	1.402	0.528	6.320
%	-1.635	0.689	3.960	2.024	0.624	6.320
	-1.327	0.787	3.960	2.663	0.627	6.320
	-0.961	0.784	3.960	3.312	0.576	6.320
	-1.612	0.000	5.940	0.308	0.000	8.820
	-1.527	0.201	5.940	0.715	0.312	8.820
60	-1.422	0.378	5.940	1.152	0.527	8.820
%	-1.281	0.518	5.940	1.619	0.639	8.820
	-1.107	0.619	5.940	2.107	0.685	8.820
	-0.878	0.659	5.940	2.606	0.695	8.820
	-0.890	0.000	7.920	0.396	0.000	11.320
	-0.855	0.099	7.920	0.612	0.205	11.320
80	-0.815	0.193	7.920	0.851	0.362	11.320
%	-0.764	0.278	7.920	1.114	0.464	11.320
	-0.694	0.347	7.920	1.393	0.529	11.320
	-0.576	0.375	7.920	1.682	0.573	11.320
	-0.167	0.000	9.900	0.483	0.000	13.820
	-0.161	0.020	9.900	0.508	0.016	13.820
100	-0.152	0.037	9.900	0.533	0.033	13.820
%	-0.141	0.054	9.900	0.560	0.047	13.820
	-0.131	0.071	9.900	0.586	0.061	13.820
	-0.117	0.087	9.900	0.613	0.075	13.820

shown in figure 14. In the sail shape figure above the table, the section profile at 5% height is shown instead of 0% height in order to refer the input data for calculation.

Mainsail alone

Variation with Mainsail Twist Angle

Figure 15 shows the performance variation of the configuration of mainsail alone with mainsail twist angle. The experiment was performed keeping AWA as 30 degrees and mean draft as around 10%. The twist angle is defined as the angle between boom line and section chord line at 80% height.

In the figure, the twist angle ranges from 7.3 degrees to 24.4 degrees for port tack. By varying of 17.1 degrees in twist angle, the value of C_X in figure (b) changes from 0.14 to 0.30 (114%), and C_Y from 1.20 to 1.54 (28%). It should be noted that the sail area for the non-dimensionalization in this case is 33.2m^2, which is 56% of the case of mainsail with 130% jib. In the small twist angle range, the value of C_D exceeds 0.5. This might be caused by the generation of wide flow separation on the mainsail surface. Since the AWA and mainsail trimming are almost same as the case of twist test with 130% jib, this result clearly indicates the jib effect on decreasing of flow separation on the mainsail. In this case, the calculated results of C_L by VLM show higher value due to not taking the flow separation into account. On the other hand, the results by RANS-based CFD become quite low value. In the figure (c), the x and z coordinates of GCE for this configuration are 1.84m backward and 5.82m upward from the origin, respectively. The experimental data are close to these values.

Figure 16 shows the calculated results of RANS-based CFD. The figure (1) indicates ID 9807172B (twist angle= 10.9 deg.), and (2) indicates 9807172F (twist angle= 24.4 deg.). It is seen that the almost streamlines of the suction side of both cases indicate flow separation. This is the reason of quite low value of C_L. Table 7 shows the shapes and three-dimensional coordinates of the sail for the cases of (1) and (2), which correspond to the calculated results shown in figure 16.

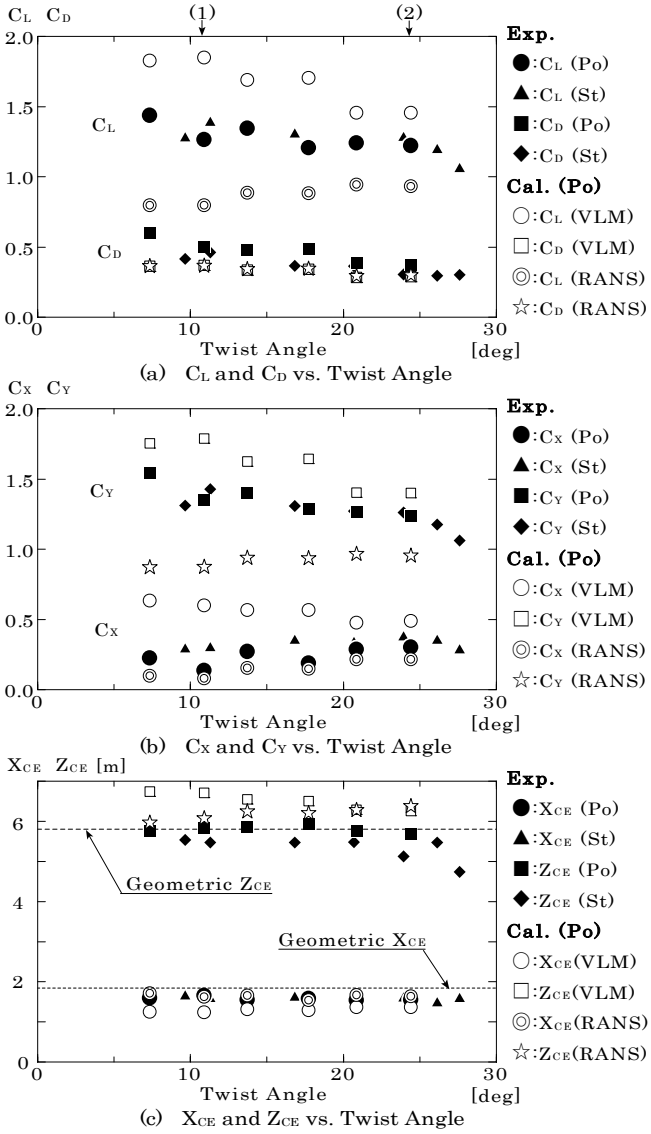

Fig.15 Performance variation with mainsail twist angle for mainsail alone

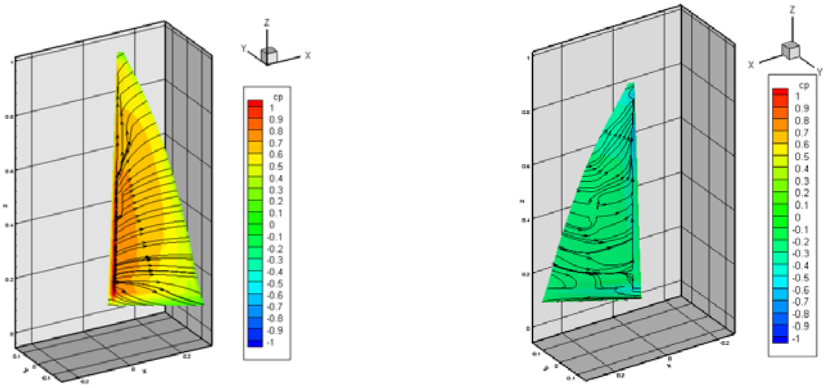

Fig. 16 (1) Comparison of surface pressure and streamlines obtained by RANS-based CFD at experimental ID 9807172B (twist angle= 10.9 deg.)

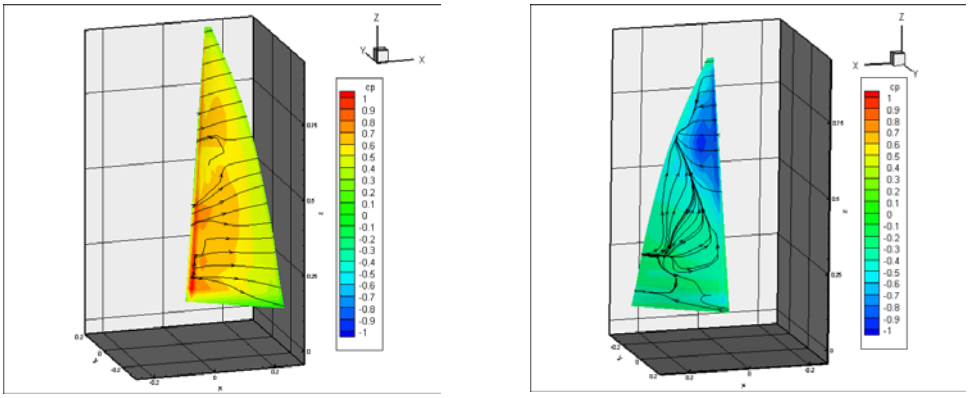

Fig. 16 (2) Comparison of surface pressure and streamlines obtained by RANS-based CFD at experimental ID 9807172F (twist angle= 24.4 deg.)

Table 7 Sail shapes, measured experimental data and three-dimensional coordinates of the sails for the cases of (1) 9807172B and (2) 9807172F

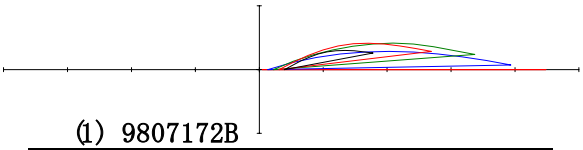

(1) 9807172B

AWA[ ]	TWIST[ ]	DRAFT[%]	AWS[m/s]	HEEL[ ]	VB[kt]
-29.88	10.88	9.26	7.19	8.72	4.24
CL	CD	CX	CY	XCE[m]	ZCE[m]
1.266	0.502	0.136	1.349	1.660	5.834

%of heit				Mainsail		
	x	y	z	x	y	z
0 %				0.046	0.000	1.320
				0.934	0.000	1.320
				1.822	0.000	1.320
				2.710	0.000	1.320
				3.598	0.000	1.320
				4.486	0.000	1.320
20 %				0.133	0.000	3.820
				0.891	0.190	3.820
				1.650	0.274	3.820
				2.411	0.274	3.820
				3.173	0.200	3.820
	Without Jib			3.937	0.072	3.820
40 %				0.221	0.000	6.320
				0.837	0.231	6.320
				1.461	0.364	6.320
				2.091	0.417	6.320
				2.730	0.357	6.320
				3.373	0.236	6.320
60 %				0.308	0.000	8.820
				0.765	0.223	8.820
				1.231	0.370	8.820
				1.710	0.414	8.820
				2.199	0.370	8.820
				2.693	0.284	8.820
80 %				0.396	0.000	11.320
				0.656	0.138	11.320
				0.923	0.244	11.320
				1.199	0.297	11.320
				1.487	0.293	11.320
				1.780	0.261	11.320
100 %				0.483	0.000	13.820
				0.512	0.009	13.820
				0.540	0.018	13.820
				0.569	0.025	13.820
				0.599	0.031	13.820
				0.628	0.038	13.820

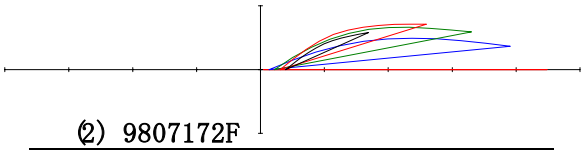

(2) 9807172F

AWA[ ]	TWIST[ ]	DRAFT[%]	AWS[m/s]	HEEL[ ]	VB[kt]
-30.53	24.41	9.70	7.27	8.79	5.25
CL	CD	CX	CY	XCE[m]	ZCE[m]
1.222	0.371	0.302	1.242	1.552	5.686

%of heit				Mainsail		
	x	y	z	x	y	z
0 %				0.046	0.000	1.320
				0.934	0.000	1.320
				1.822	0.000	1.320
				2.710	0.000	1.320
				3.598	0.000	1.320
				4.486	0.000	1.320
20 %				0.133	0.000	3.820
				0.869	0.276	3.820
				1.615	0.443	3.820
				2.372	0.492	3.820
				3.138	0.453	3.820
	Without Jib			3.908	0.365	3.820
40 %				0.221	0.000	6.320
				0.793	0.349	6.320
				1.389	0.569	6.320
				2.010	0.660	6.320
				2.651	0.648	6.320
				3.301	0.590	6.320
60 %				0.308	0.000	8.820
				0.712	0.315	8.820
				1.141	0.549	8.820
				1.607	0.664	8.820
				2.095	0.707	8.820
				2.595	0.712	8.820
80 %				0.396	0.000	11.320
				0.626	0.181	11.320
				0.867	0.338	11.320
				1.126	0.454	11.320
				1.405	0.527	11.320
				1.692	0.580	11.320
100 %				0.483	0.000	13.820
				0.508	0.016	13.820
				0.534	0.032	13.820
				0.560	0.047	13.820
				0.586	0.061	13.820
				0.613	0.075	13.820

CONSIDERATION OF RESULTS BY RANS-BASED CFD

Main aspects of the present flow fields are dominated by multiple-lifting-surface aerodynamic interactions. Especially for larger AWA, a large-scale flow separation in the leeward side of sails is also involved. In general, complex vortex generation in the wake is seen especially near the top and bottom of the sails, i.e., tip vortices are clearly interacted and influenced by boundary layer flows on sails. Resultant aerodynamic forces are mostly dominated by the pressure component, while the contribution of the frictional component is generally small. Challenges in RANS-based CFD is the accurate prediction of boundary layer flows on sails and three-dimensional flow separation, which is associated with the above-mentioned vortex generation. Geometrical complexities yield another aspect of CFD challenges. Accuracy in predicted CE is also of great interest, in association with correct prediction of the above-mentioned three-dimensional flow separation.

Through the analyses of the results, it appears that the overall trends of flow and aerodynamic forces shown in the measurements are fairly well captured in the present computations. It is also seen that the multi-block domain decomposition considered here is very effective for the present mainsail and jib configurations. The present automatic gridding scheme successfully generates high-quality structured grids for various sail geometries, AWA, and heel angles considered in the present study. Although the advantages of a structured grid system for high-resolution in boundary layer flow is highlighted, building a grid in this fashion is difficult to apply to complex geometry. This is apparently resolved by the present scheme. Besides, any numerical instability has not been experienced in all series computations presented here, which is in no doubt due to the sufficiently high quality of the present computational grid.

INFLUENCE OF CFD TECHNIQUE ON PERFORMANCE

Influence of Turbulence Models and Mesh Size

As recent advancement of information technology continuously expands capability of CFD, the RANS-based CFD has matured to the point where it is widely accepted as a key tool for predicting ship boundary layer and wake flows. However, the choice of an appropriate turbulence model is still a point of concern, as that has been a long-lasting issue discussed in CFD workshops since 1980's (most recently, Hino, 2005). The selection of sufficiently accurate mathematical model must depend on complexities of flow to be resolved. In prediction of thin boundary layer flow, the emphasis will be on relatively simple models that provide results with low computational costs; however, more complex models will be required for detailed prediction of thick boundary layer and wake flows.

In development of the present RANS-based CFD code, turbulence model associated with the near-wall flow model has carefully been evaluated by the author. An initial motivation of the work is to investigate appropriate turbulence model for accurate prediction of boundary-layer and wake flows, number of grids must be located in the boundary layer, and a way to overcome one of difficulties many RANS codes often suffer, i.e., Rn limitation. The

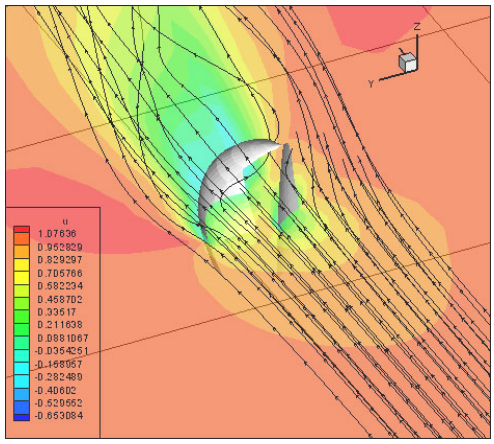

Fig.17 Overview of flow field around the mainsail/ spinnaker configuration.

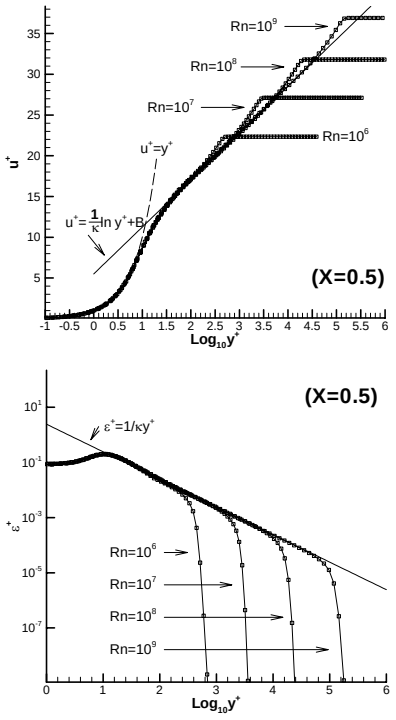

Fig.18 Comparison of near-wall profiles of velocity and turbulent quantities (flat-plate flow). Two-layer k-ε model results.

author found that even a Navier-Stokes equation solver is capable for predicting large-scale separation flows and associated aerodynamic forces with practical accuracy if a sufficiently large number of computational grids are used (Tahara, Hayashi, 2003, see Fig.17). However, for cases where high resolution of turbulent boundary layer is crucial, as for the present upwind sail system, an appropriate turbulence model with correctly located near-wall grids is necessary.

Fig. 18 shows comparison of flat-plate near-wall profiles of velocity for model to ship full scale Rn, where it appears that logarithmic region clearly increases as Rn increases. In general, near wall grid spacing must be around $y^+=1$, which is also confirmed by others who performed similar investigations (e.g., CFD workshop, Hino, 2005). If sufficiently high-resolution computational grid is used (e.g., a half million), relatively simple turbulence model is capable to accurately predict hydrodynamic forces. Based on these precursory results, the fact that the total number of grids used was more than a half million, the expected character of flow around upwind sails, and in consideration of computational costs for many case studies, an algebraic turbulence model (Baldwin-Lomax Model) was selected.

Influence of Mast on Aerodynamic Forces and Flow

The present RANS-based CFD method was applied for evaluation of mast influences on aerodynamic forces and flow. Focus here is particularly placed on a configuration in twist series data, i.e., experimental ID 97072218 (AWA 31.67 deg. Heel angle 13.44 deg., and Twist 24.13%). Fig.19 shows computational geometries of mainsail, jib and mast configuration. For the present study, all surface data are represented by IGES data. Then, the data are used for multi-block grid generation by using a commercial software GRIDGEN v.15 (Pointwise, Inc.). Application of this software is found very effective to investigate appropriate grid topology and resolution. In future work, the gridding procedure will be fully automated.

For correct representation of mast geometry, number of computational grids and multi-blocks are slightly increased, i.e., around 700,000 grid points and 52 blocks are used. Both grids for with-mast and without-mast cases are generated with careful consideration to minimize grid-dependency on results, so that the same grid number and blocks are used for the two cases. Overall grid quality is similar to that for the earlier-discussed series calculations, which is supported by a fact that differences in x_{CE}, z_{CE}, C_L, and C_D for without mast case between the present and the series calculation is all less than 0.5%. Converged solutions are obtained within 2000 RANS global iterations, i.e., 20 non-dimensional time. This is similar convergence trend as that for the series calculations.

Fig. 20 shows comparison of CE and aerodynamic forces. In the figure, "W. Mast" and "W/O Mast" correspond to with-mast and without-mast cases, respectively. In addition, Figs.21 and 22 show sail surface pressure and streamlines, and stream ribbons in flow field to identify salient influence of mast on flow through comparison of the two cases. Furthermore, local flow field in horizontal cross section at Z=0.5 (i.e., horizontal midsection of mainsail) is shown in Fig.23. Note that the present computation simulates port-tack sailing, therefore, the port and starboard sides correspond to the pressure and suction sides, respectively.

It is seen in the present results that influence of mast on flow is particularly significant in the mast-wake region. Due to the limited grid resolution, the details of the Karman vortex shedding occurs on the mast surface are captured with limited accuracy, but gross feature of the influences on downward flow is found well reproduced. Surface streamlines on mainsail indicate complex three-dimensional separation in the mast-wake region, which is more obvious on pressure side surface. In spite of the redirection of surface streamlines, general features of the surface pressure distributions on mainsail are similar to those for without-mast case. Influences of mast on flows below the mainsail is more purely due to the Karman vortex shedding from the mast surface, and directly leads to increase of drag force. Due to inclusion of mast, C_D is increased in about 11%, and the resultant value is closer to the experimental data. Differences in C_L and z_{CE} are less that 1% and these may be judged insignificant. The x_{CE} slightly moved backward in about 10%, and the resultant value is closer to the measurements.

In summary, as far as the present sail configuration and sailing conditions are concerned, predicted trends in solutions for with-mast case indicate many improvements over the results for without-mast case. The configuration is more realistic, and will be effective for more accurate prediction of flow and aerodynamic forces. Needs of special care on computational grids may be a drawback; however, increasing power of computer will reduce limitation of grid size, and further grid refinement to capture more detailed Karman vortex shedding on mast will be easier in near future. As the earlier-mentioned, automatic gridding will be realized in future work.

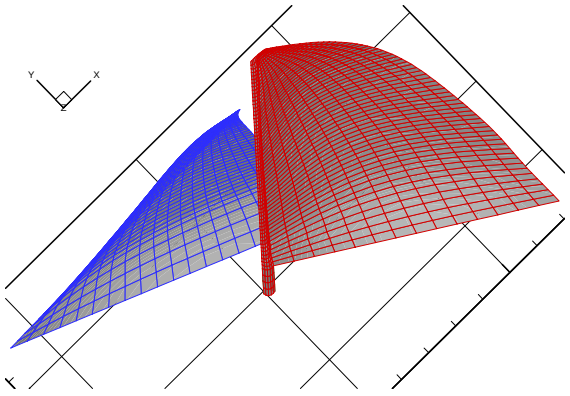

Fig.19 Overview of sail surface grids including mast geometry. All surfaces are defined in IGES format

data.

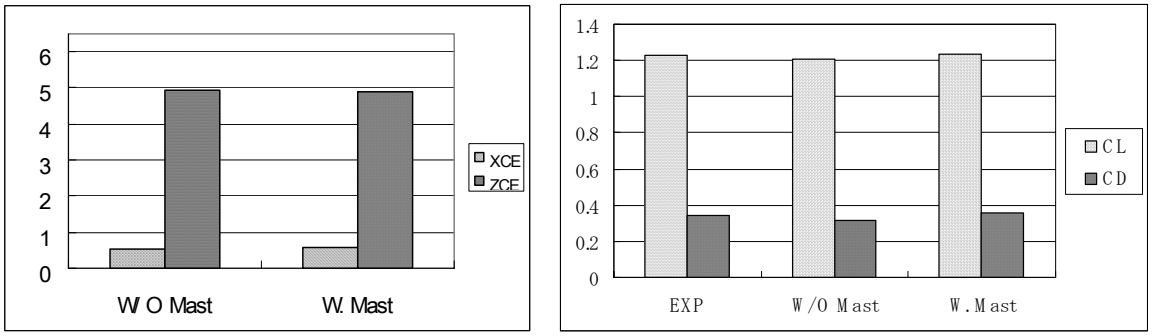

Fig.20 Comparison of aerodynamic forces and center of effort. Left: comparison of x_{CE} and z_{CE}; and Right: comparison of C_L and C_D, respectively. "W. Mast" and "W/O Mast" in the figure correspond to with-mast and without-mast cases, respectively.

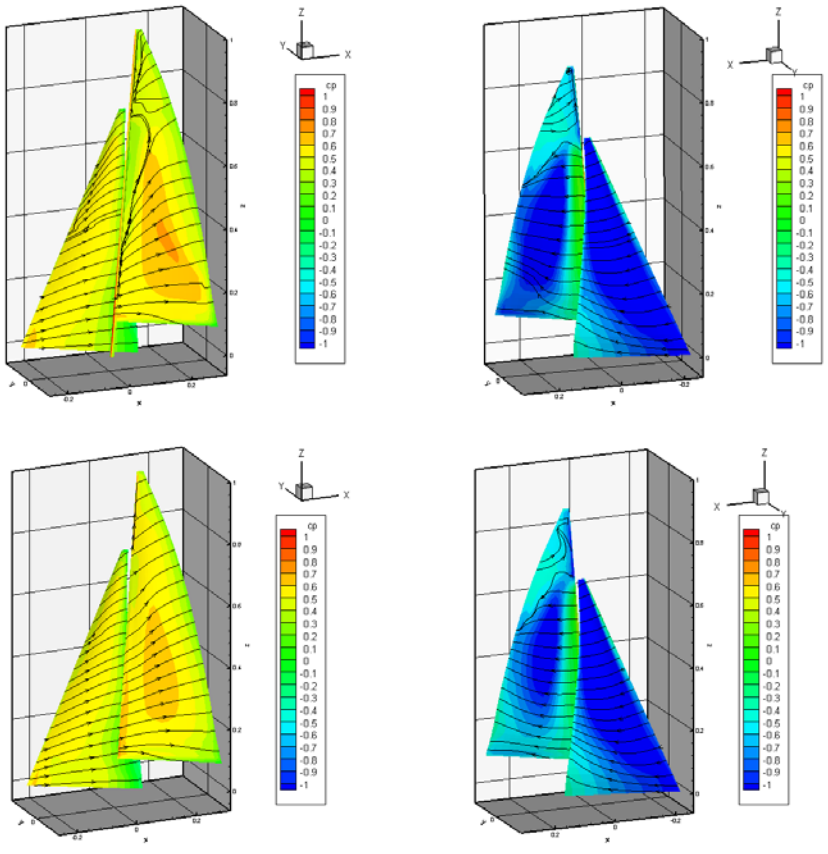

Fig.21 Comparison of surface pressure and streamlines between with-mast and without-mast cases. Left and right columns correspond to the port and starboard sides, i.e., pressure and suction sides, respectively.

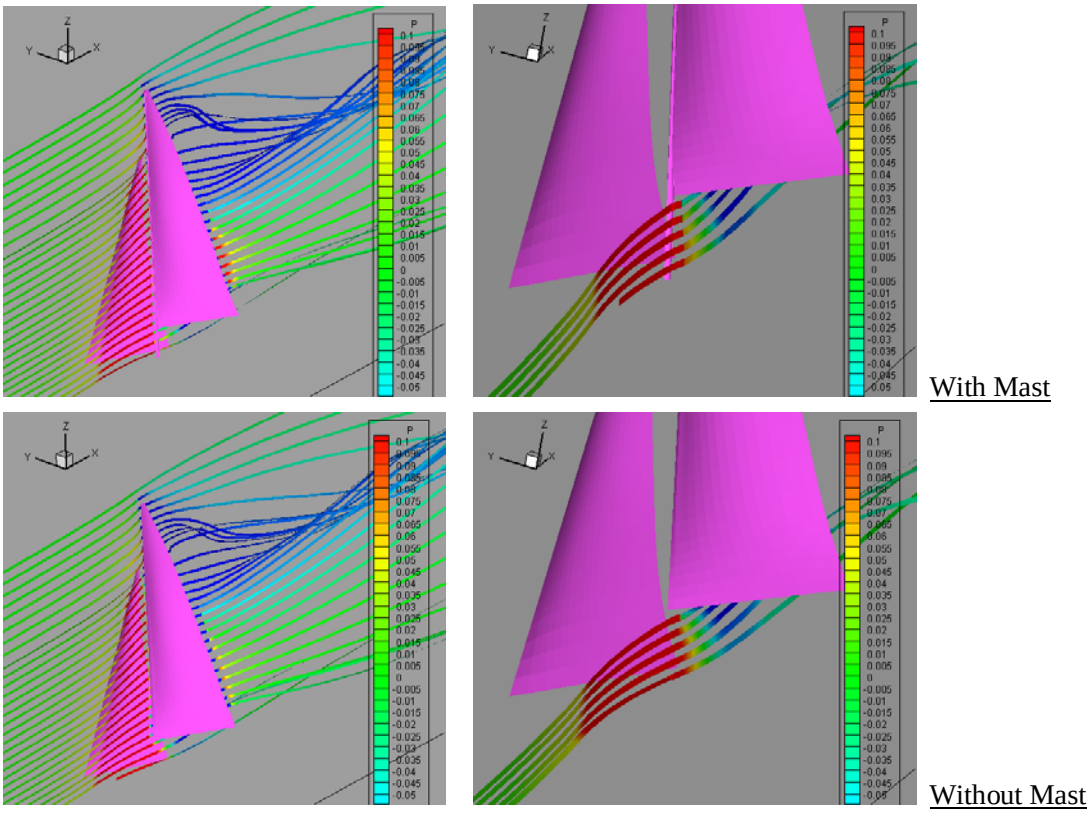

Fig.22 Comparison of stream ribbons between with-mast and without-mast cases. Left and right columns correspond to global and local views, respectively.

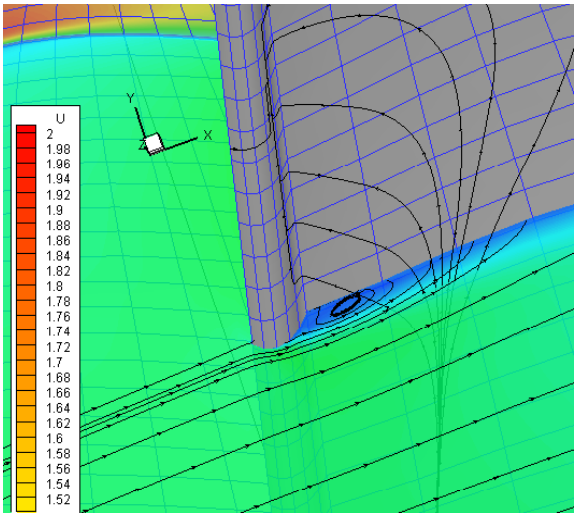

Fig.23 Surface streamlines on mainsail and in horizontal cross section (z=0.5, midsection of mainsail). With-mast case.

CONCLUSIONS

The sail shapes and performance of IMS type sails are measured using a sail dynamometer boat *Fujin* for upwind condition. The tested sail configurations are as follows: mainsail with 130% jib, mainsail with 75% jib and mainsail alone. The three-dimensional coordinates of the sails are obtained from the measured data and tabulated with the aerodynamic coefficients.

From the experiments, the variation of sail performance such as lift and drag coefficients, and coordinates of center of effort were indicated quantitatively in full-scale with the change of AWA, mean draft of mainsail and twist angle of mainsail.

Numerical calculations are also performed using the measured sail shapes. The calculation methods are of two types; Reynolds-averaged Navier-Stokes (RANS)-based CFD and vortex lattice methods (VLM). A multi-block RANS-based CFD method developed by one of the authors was used and an automatic grid generation scheme was adopted. The computed results were compared with the measured data. For the cases of mainsail and jib, both calculated results well captured the overall trends of flow and aerodynamic forces shown in the measurements. For

the case of mainsail alone, the C_L value resulted higher in VLM and lower in RANS-based CFD than the measured. The RANS-based CFD method was also applied for evaluation of mast influence on aerodynamic forces and flow. Due to inclusion of mast, the value of C_D increased about 11% and the resultant value was closer to the experimental data. Further grid refinement to capture more detailed flow around mast and sails will be thrust in near future.

The sail shape database and comparison with numerical calculations indicated in this report will provide a good benchmark for the sail performance analysis of the upwind condition of IMS type sails.

ACKNOWLEDGEMENTS

The sail dynamometer boat *Fujin* was built for sail tests for the Japanese America's Cup challenger by the Grant-in-Aid of the Nippon Foundation. We would like to thank the Nippon Foundation for the valuable expense. We wish to express our thanks to Yamaha Motor Co. Ltd. for building *Fujin* and North Sails Japan Co. for preparing the sails. We also would like to thank Mr. H. Mitsui, the harbormaster of the Anamizu Bay Seminar House of Kanazawa Institute of Technology, for his powerful assistance on the sea tests. Help in sea tests given by graduate and undergraduate students of Kanazawa Institute of Technology is also gratefully acknowledged. The graduate students were Masaya Miyagawa, Takashi Hasegawa and Munehiko Ogihara.

REFERENCES

Fukasawa, T., "Aeroelastic Transient Response of 3-Dimensional Flexible Sail," Aero-Hydroelasticity, ICAHE'93, 1993.

Fukasawa, T. and Katori, M., "Numerical Approach to Aeroelastic Responses of Three-Dimensional Flexible Sails," 11th Chesapeake Sailing Yacht Symposium, SNAME, 1993.

Hino T (Ed.), CFD Workshop Tokyo 2005. National Maritime Research Institute, 9-11 March, Tokyo, Japan, 2005.

Hochkirch, K. and Brandt, H., "Fullscale Hydrodynamic Force Measurement on the Berlin Sailing Dynamometer," 14th Chesapeake Sailing Yacht Symposium, SNAME, 1999.

Masuyama, Y. and Fukasawa T., "Full Scale Measurement of Sail Force and the Validation of Numerical Calculation Method," 13th Chesapeake Sailing Yacht Symposium, SNAME, 1997.

Milgram, J. H., Peters, D. B. and Eckhouse, D.N., N., "Modeling IACC Sail Forces by Combining Measurements with CFD," 11th Chesapeake Sailing Yacht Sympposium, SNAME, 1993.

Tahara, Y., "A Multi-Domain Method for Calculating Boundary-Layer and Wake Flows around IACC Sailing Yacht," J. Kansai Society of Naval Architects, Japan 226: 63-76, 1996a.

Tahara Y., "Evaluation of a RaNS Equation Method for Calculating Ship Boundary Layers and Wakes Including Wave Effects," J. Society of Naval Architects of Japan 180:59-80, 1996b.

Tahara, Y., "Wave Influences on Viscous Flow around a Ship in Steady Yaw Motion," J. Society of Naval Architects of Japan 186: 157-168, 1999.

Tahara, Y., Ando, J., "Comparison of CFD and EFD for KCS Container Ship in With-out/With-Propeller Conditions," Gothenburg 2000 - A Workshop on Numerical Ship Hydrodynamics, Gothenburg, Sweden, 2000.

Tahara, Y., Hayashi, G., "Flow Analyses around Downwind-Sail System of an IACC Sailing Boat by a Multi-Block NS/RaNS Method," J. Society of Naval Architects of Japan 194:1-12, 2003.

Tahara, Y., Stern, F., Himeno,, "Y. Computational Fluid Dynamics-Based Optimization of a Surface Combatant," J. Ship Research 48(4): 273-287, 2004.

Tahara, Y., "Development and Demonstration of Simulation Based Design for Parachute Aerodynamic Design," 7th International Conference on Hydrodynamics, Ischia, Italy, 2006.

Tahara, Y., Tohyama, S., Katsui, T., "CFD-Based Multi-Objective Optimization Method for Ship Design," To appear International J. Numerical Methods in Fluids, 2006.

Tahara, Y., Wilson, R., Carrica, P., Stern, F., "RANS Simulation of a Container Ship Using a Single-Phase Level Set Method with Overset Grids and Prognosis for Extension to Self-Propulsion Simulator," To appear J. Marine Science and Technology, 2006.